Supplementary Information for:

Synthesis, characterization, and electrochemical properties of a first-row metal phthalocyanine series

Madeline Peterson,† Camden Hunt,† Zongheng Wang, Shannon E. Heinrich, Guang Wu, and Gabriel Ménard*

Department of Chemistry and Biochemistry, University of California, Santa Barbara, California 93106, United States

Table of Contents

1. NMR Spectra

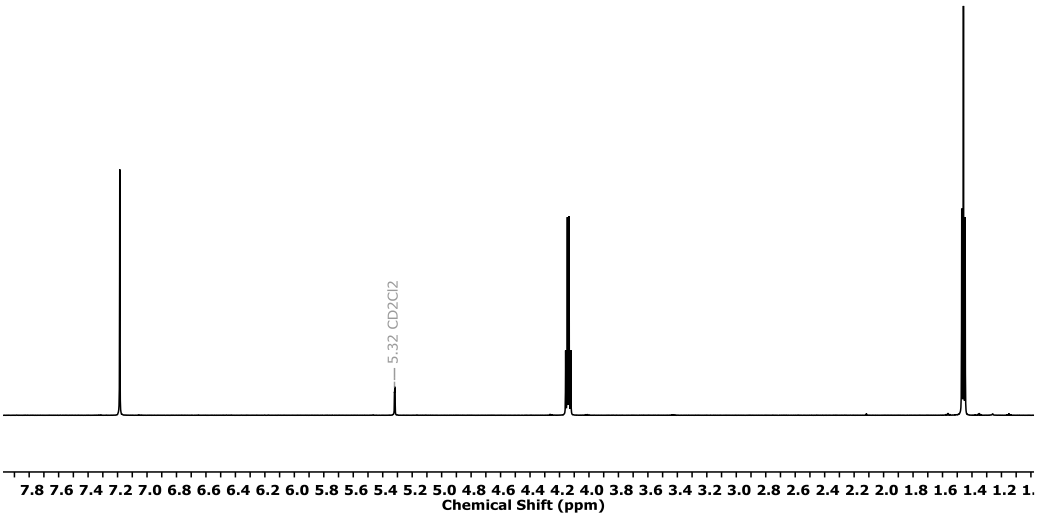

Figure S1. ^{1}H NMR spectrum of 3,6-Diethoxyphthalonitrile, taken in CD_2Cl_2.

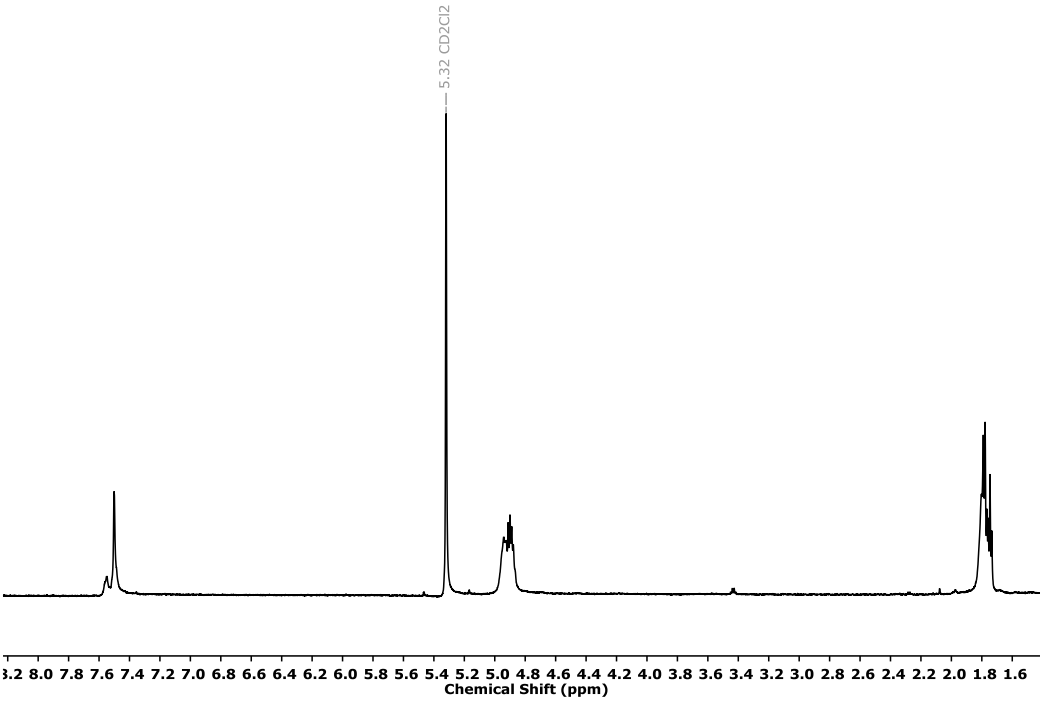

Figure S2. ^{1}H NMR spectrum of $^{\mathbf{EtO}}$**PcHLi**, taken in CD_2Cl_2.

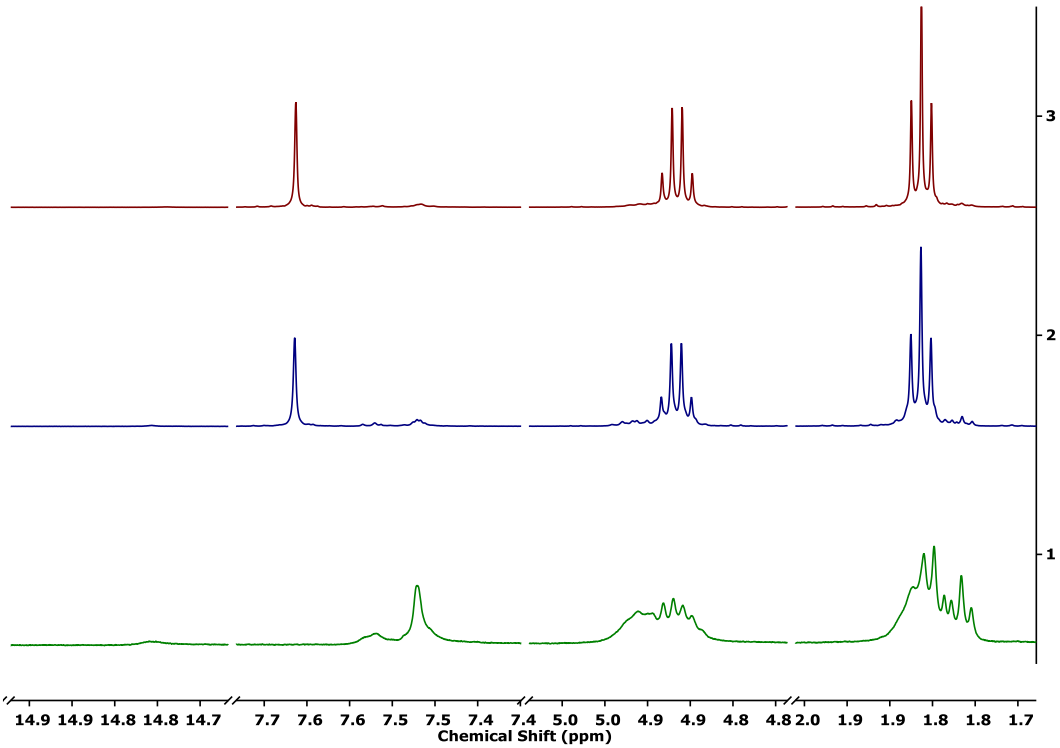

Figure S3. ^{1}H NMR spectra with relevant regions illustrating the HCl-induced conversion of ^{EtO}**PcHLi** to ^{EtO}**PcH$_2$** over 48 h, taken in CD_2Cl_2; 1) t = 0; 2) t = 24 h; 3) t = 48 h.

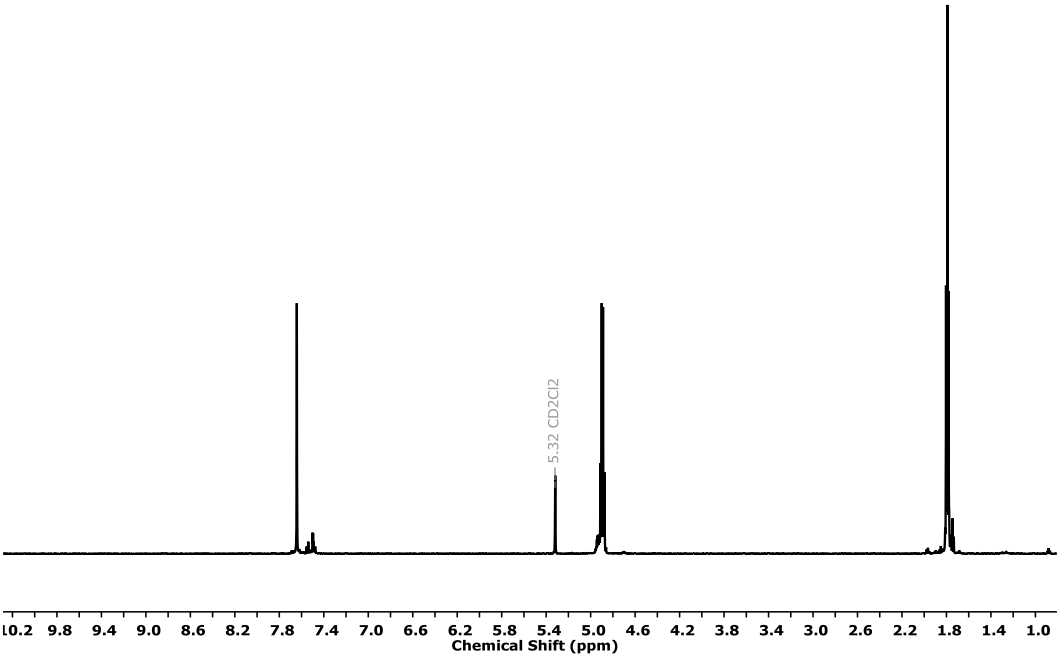

Figure S4. ^{1}H NMR spectrum of ^{EtO}**PcH$_2$**, taken in CD_2Cl_2.

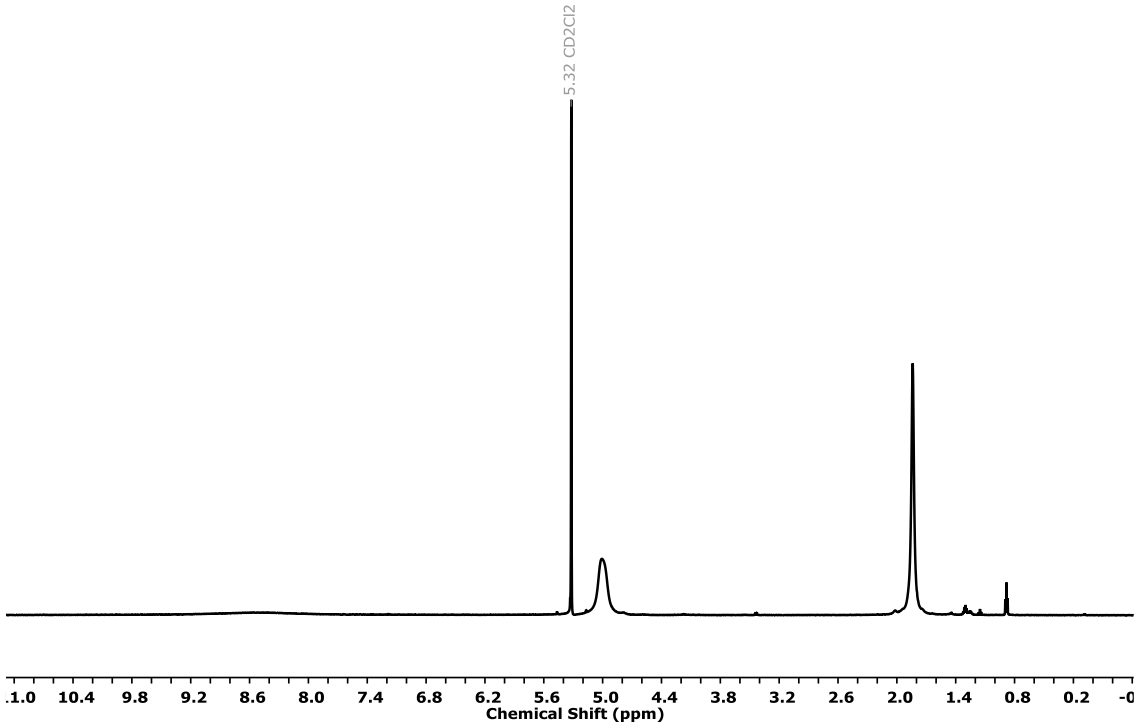

Figure S5. ^{1}H NMR spectrum of ^{EtO}**PcVO**, taken in CD_2Cl_2.

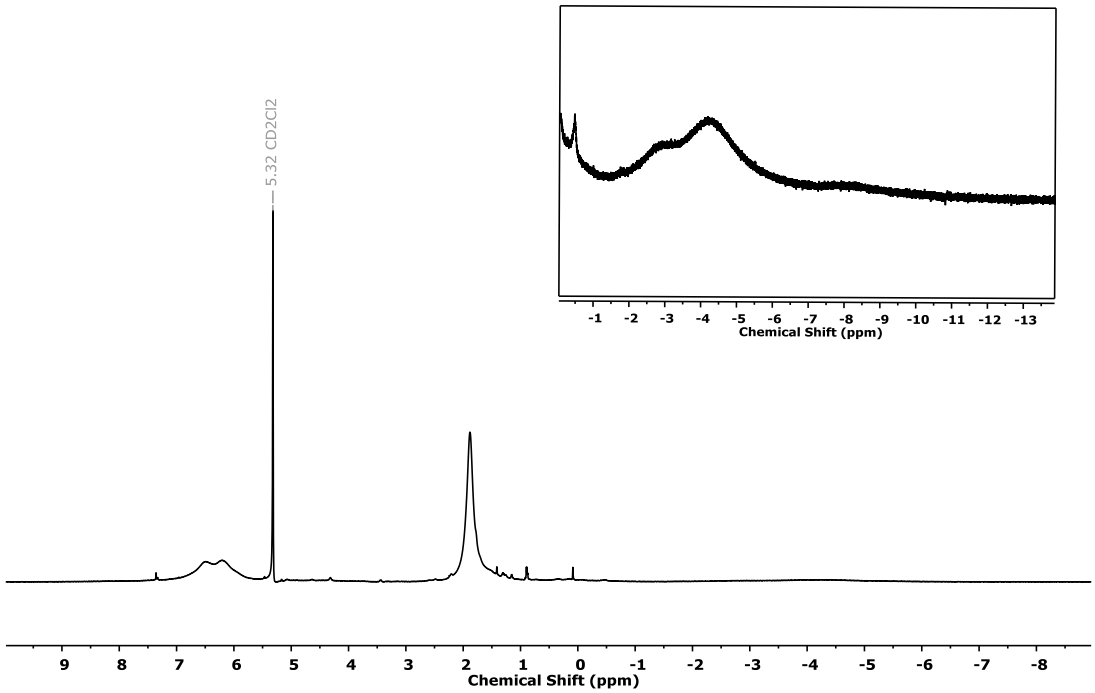

Figure S6. ^{1}H NMR spectrum of ^{EtO}**PcCr**, taken in CD_2Cl_2.

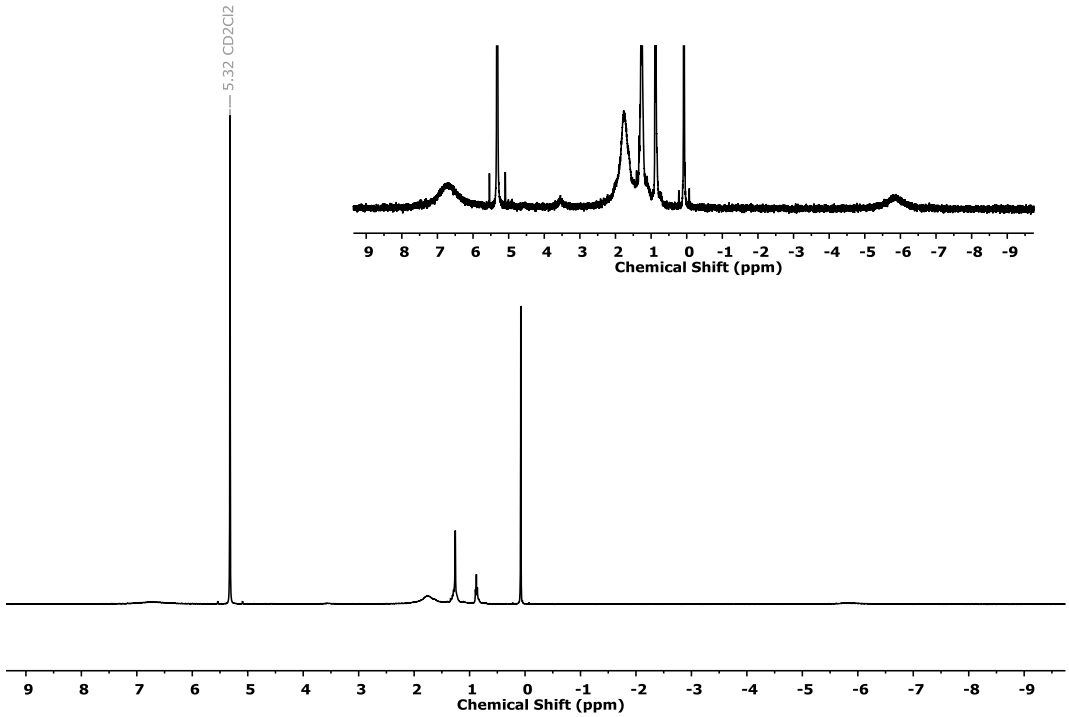

Figure S7. ^{1}H NMR spectrum of ^{EtO}**PcMnCl**, taken in CD_2Cl_2.

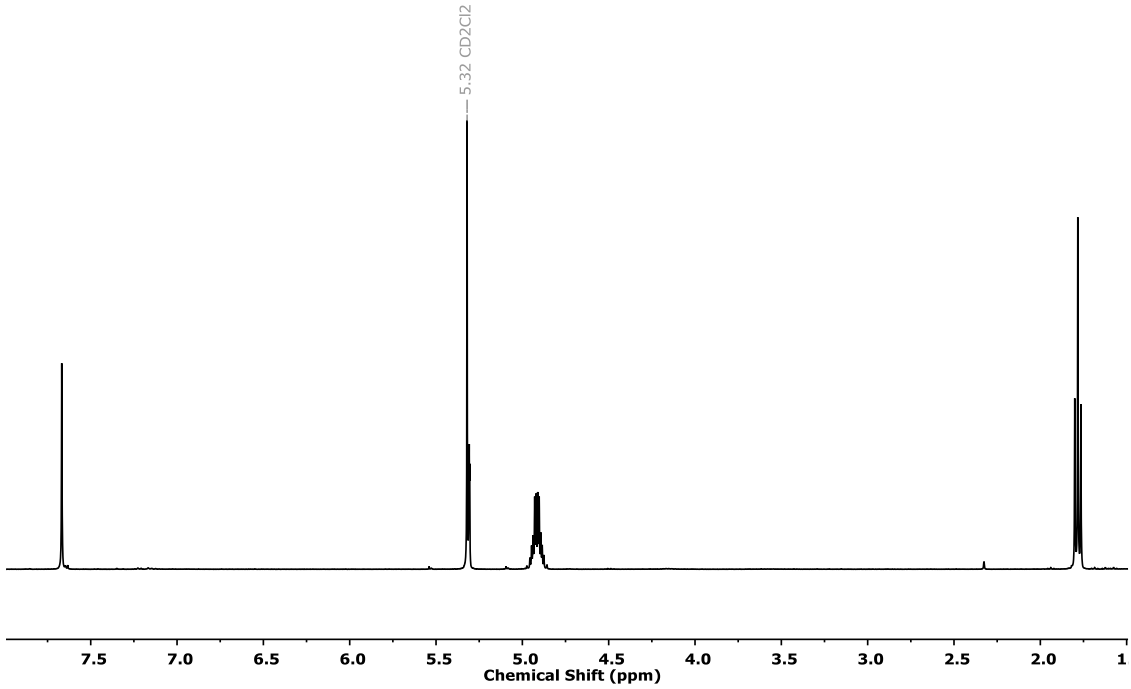

Figure S8. ^{1}H NMR spectrum of ^{EtO}**PcMnN**, taken in CD_2Cl_2.

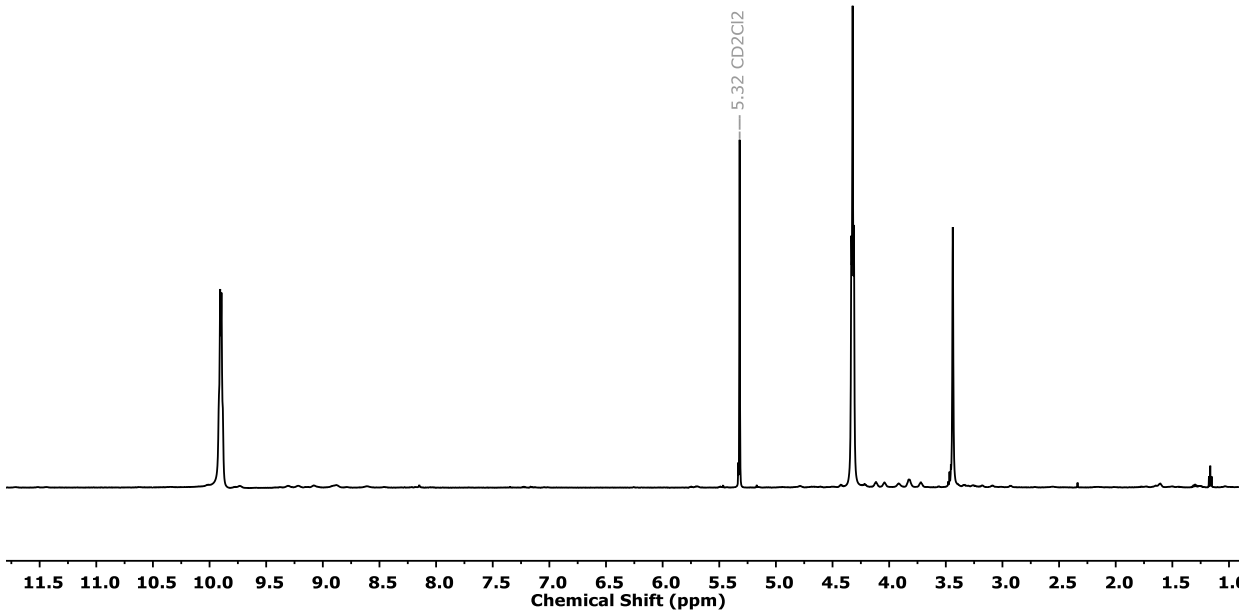

Figure S9. ^{1}H NMR spectrum of ^{EtO}**PcFe**, taken in CD_2Cl_2.

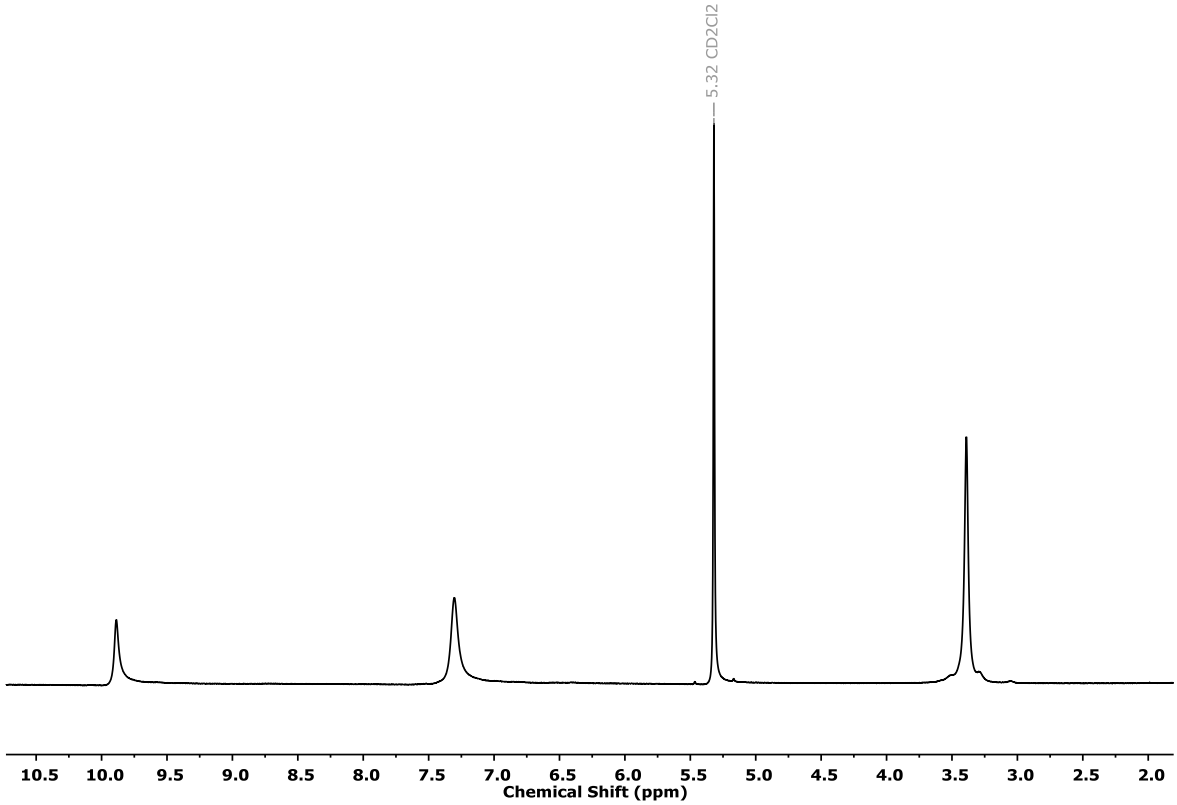

Figure S10. ^{1}H NMR spectrum of ^{EtO}**PcCo**, taken in CD_2Cl_2.

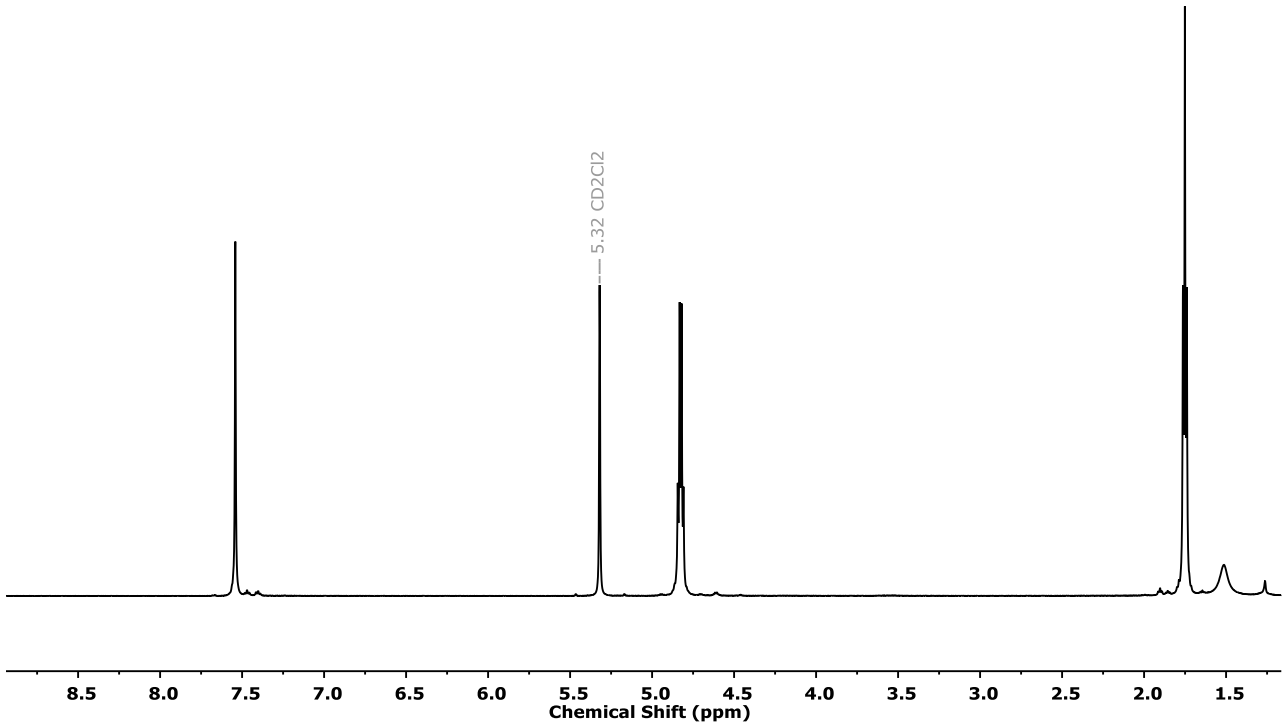

Figure S11. ^{1}H NMR spectrum of ^{EtO}**PcNi**, taken in CD_2Cl_2.

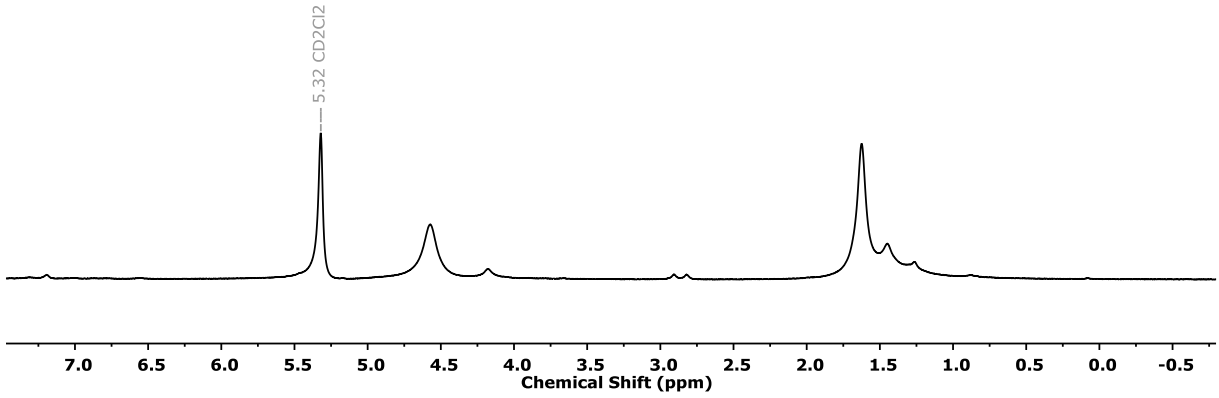

Figure S12. ^{1}H NMR spectrum of ^{EtO}**PcCu**, taken in CD_2Cl_2.

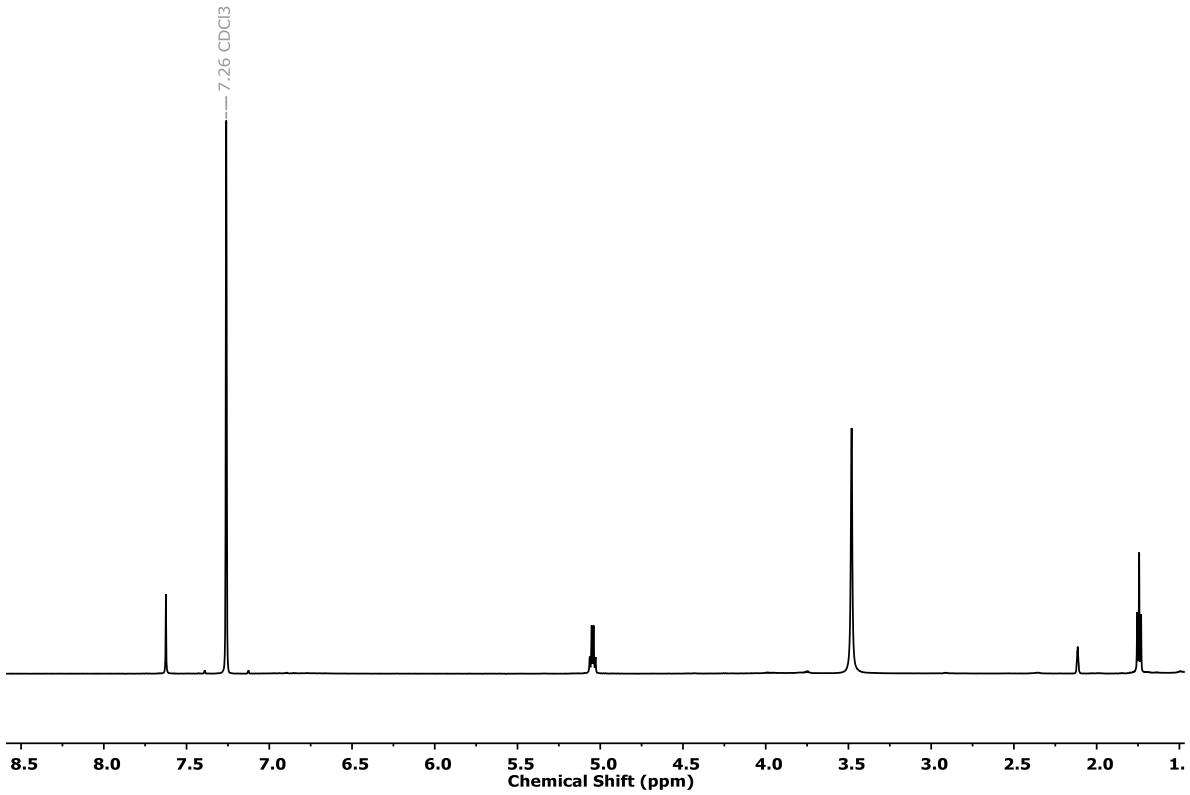

Figure S13. ^{1}H NMR spectrum of $^{\mathbf{EtO}}$**PcZn**, taken in $CDCl_3$.

2. EPR Spectra

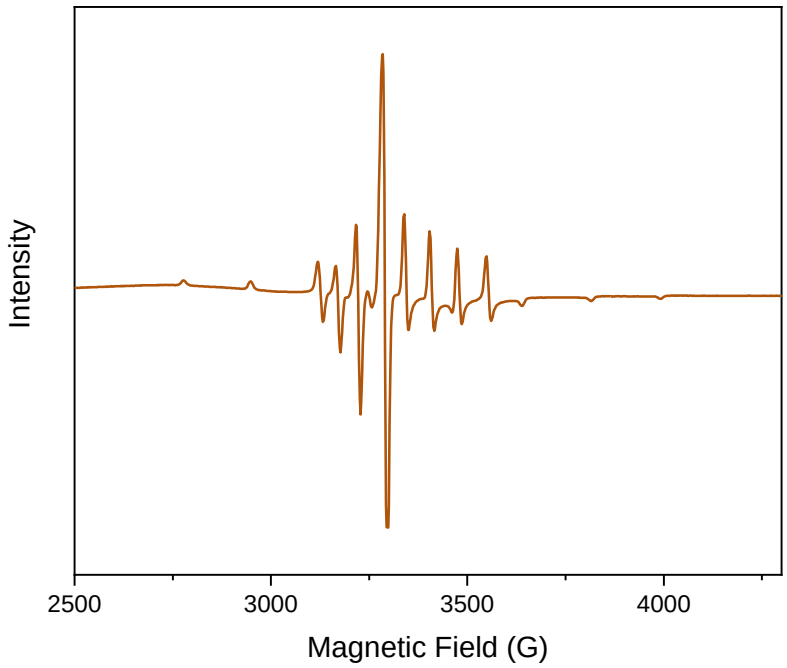

Figure S14. X-band EPR (ν = 9.302510 GHz) spectrum of ^{EtO}**PcVO** taken in CH_2Cl_2 at 100K.

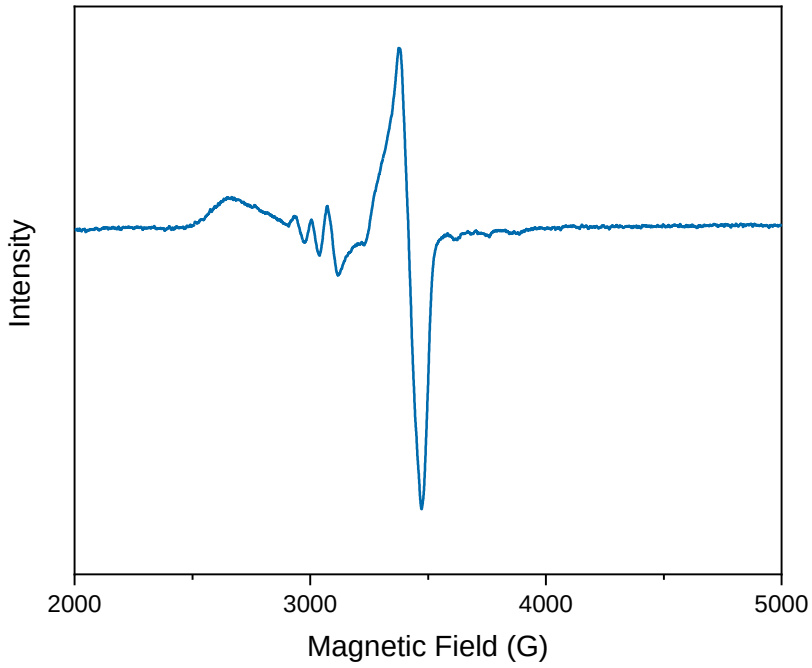

Figure S15. X-band EPR (ν = 9.606425 GHz) spectrum of ^{EtO}**PcCo** taken in CH_2Cl_2 at 100K.

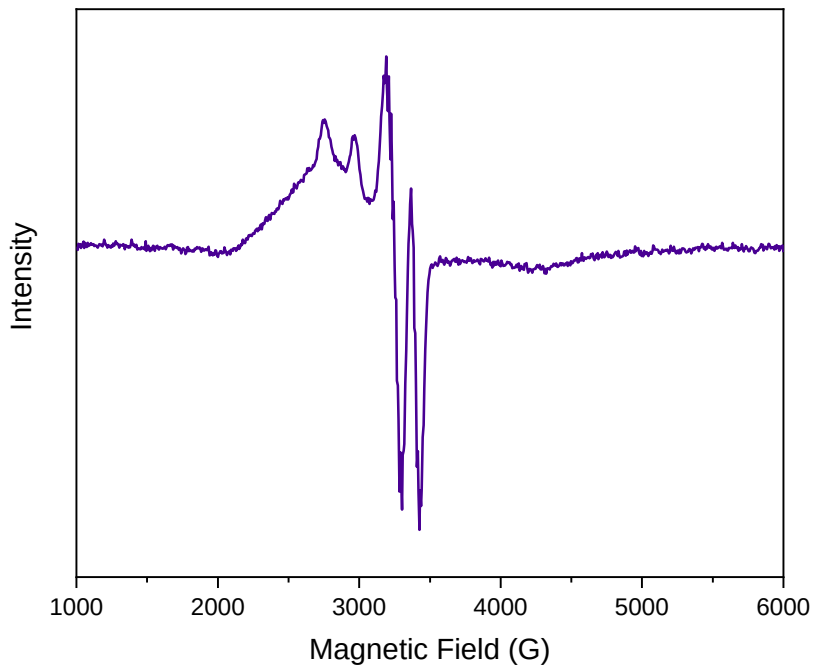

Figure S16. X-band EPR(ν = 9.292836 GHz) spectrum of ^{EtO}**PcCu** taken in CH_2Cl_2 at 100K.

3. UV-Vis Spectra

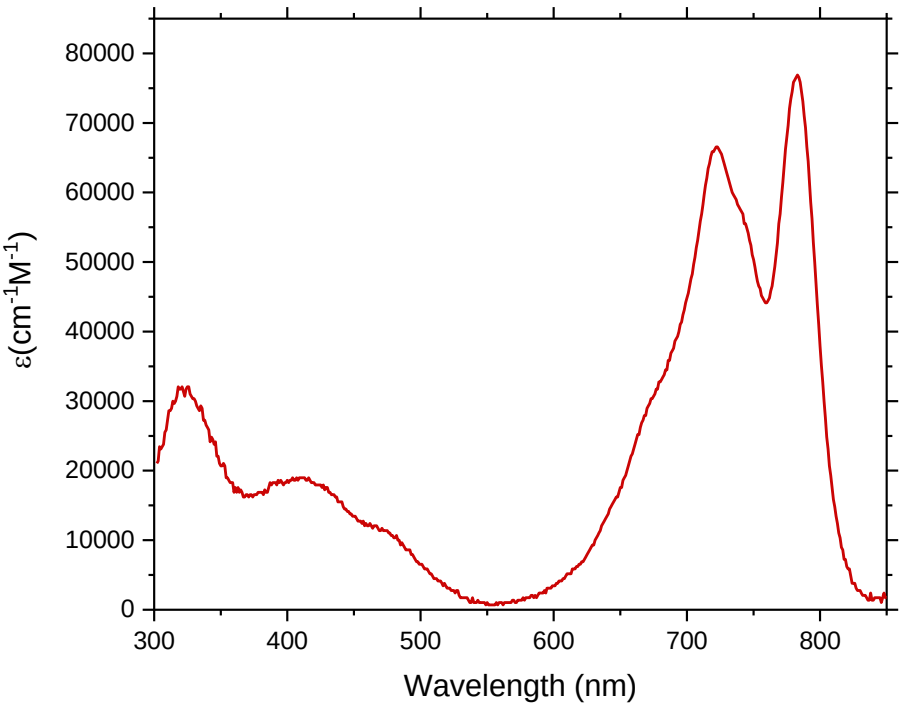

Figure S17. UV-Vis spectrum of ^{EtO}**PcHLi** taken in CH_2Cl_2 (2.9 μM).

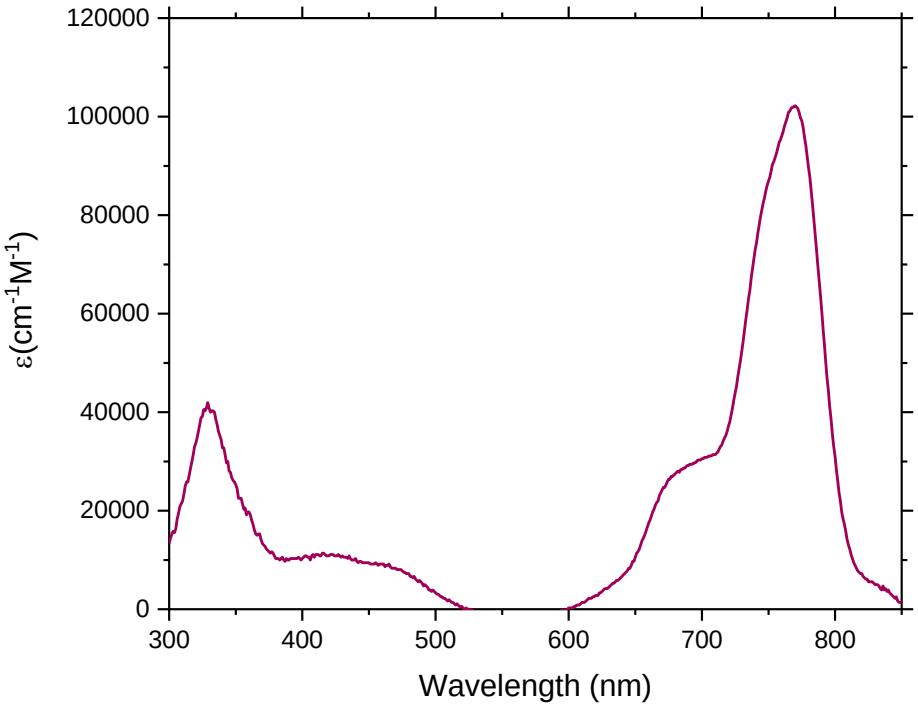

Figure S18. UV-Vis spectrum of ^{EtO}**PcH$_2$** taken in CH_2Cl_2 (3.6 μM).

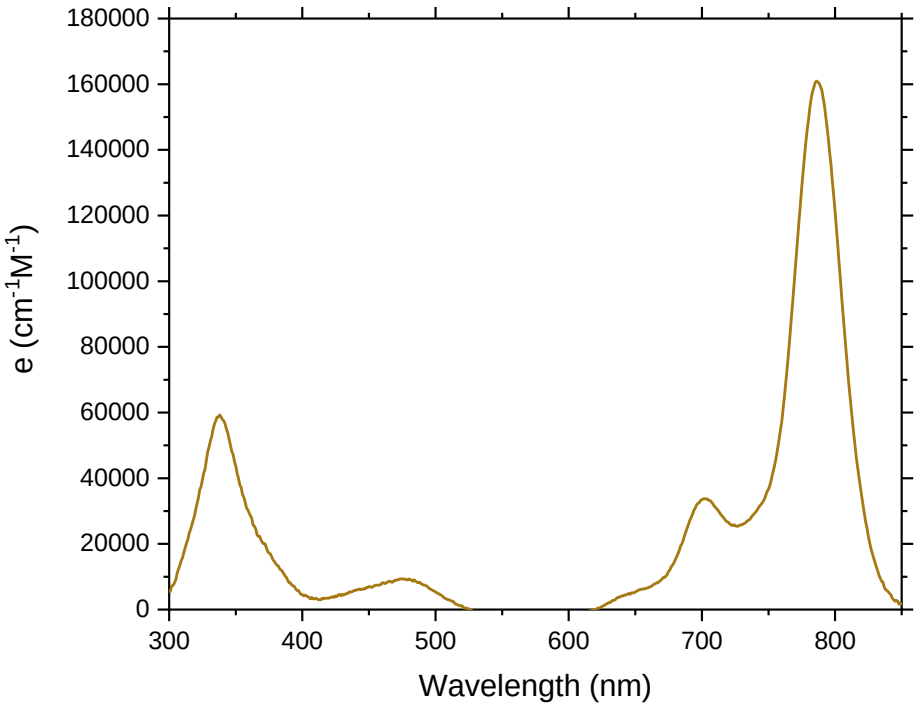

Figure S19. UV-Vis spectrum of ^{EtO}**PcVO** taken in CH_2Cl_2 (4.3 μM).

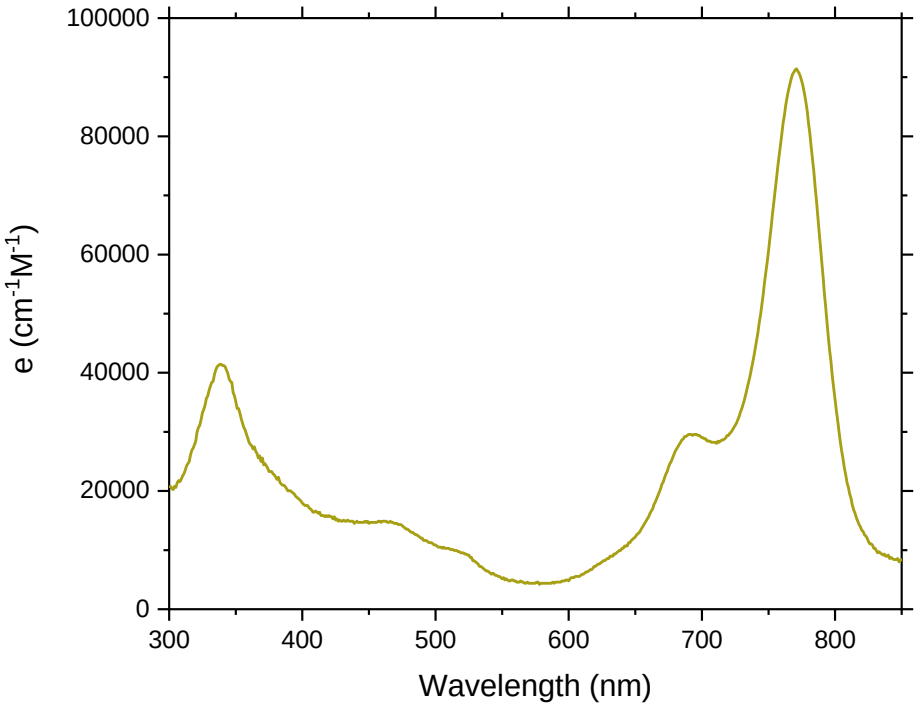

Figure S20. UV-Vis spectrum of ^{EtO}**PcCr** taken in CH_2Cl_2 (5.2 μM).

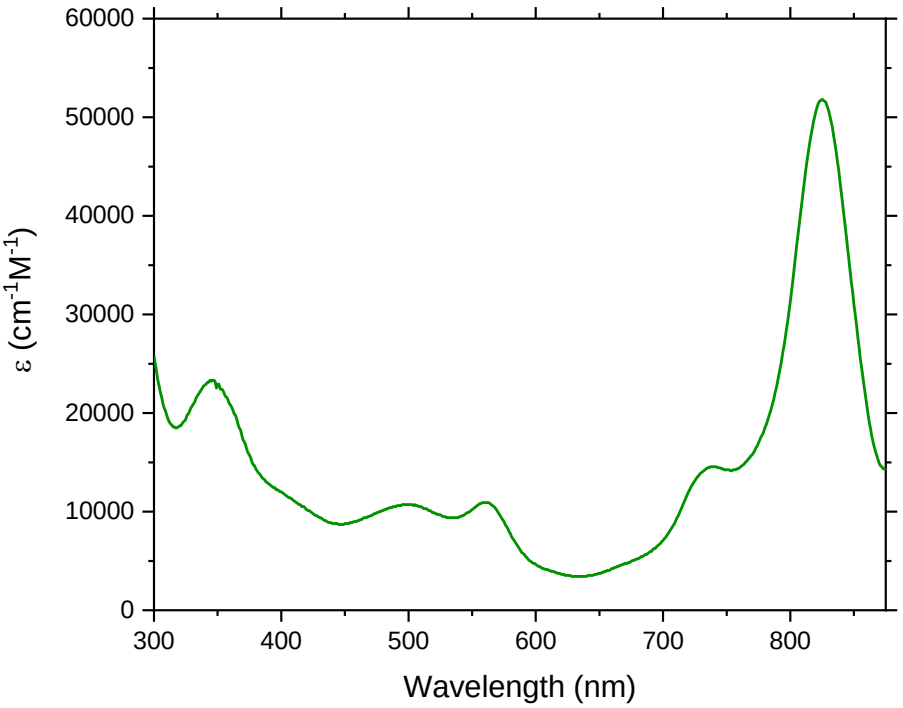

Figure S21. UV-Vis spectrum of ^{EtO}**PcMnCl** taken in CH_2Cl_2 (9.9 μM).

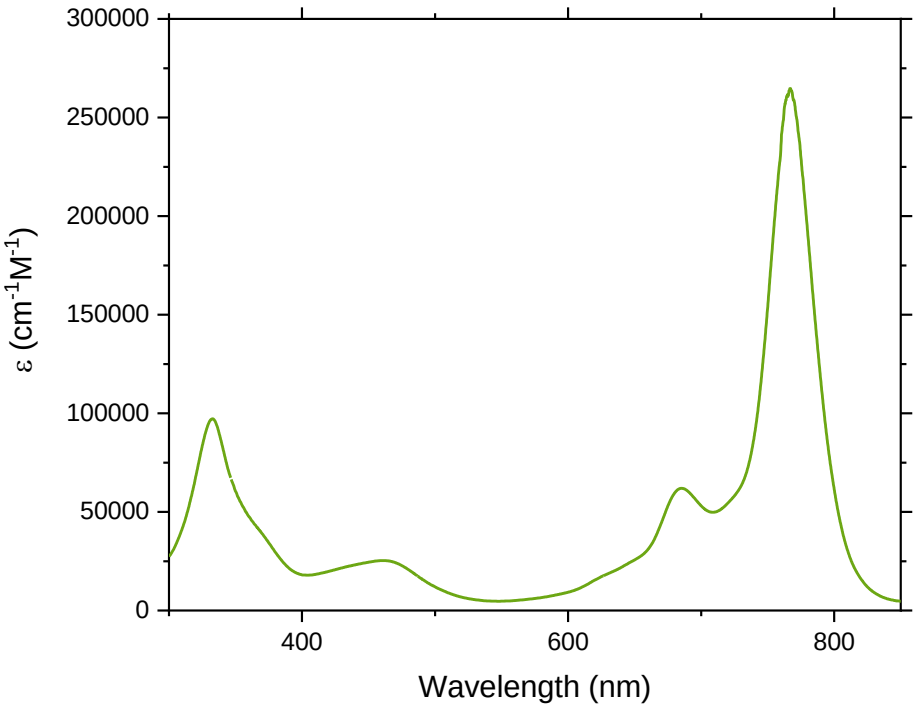

Figure S22. UV-Vis spectrum of ^{EtO}**PcMnN** taken in CH_2Cl_2 (3.4 μM).

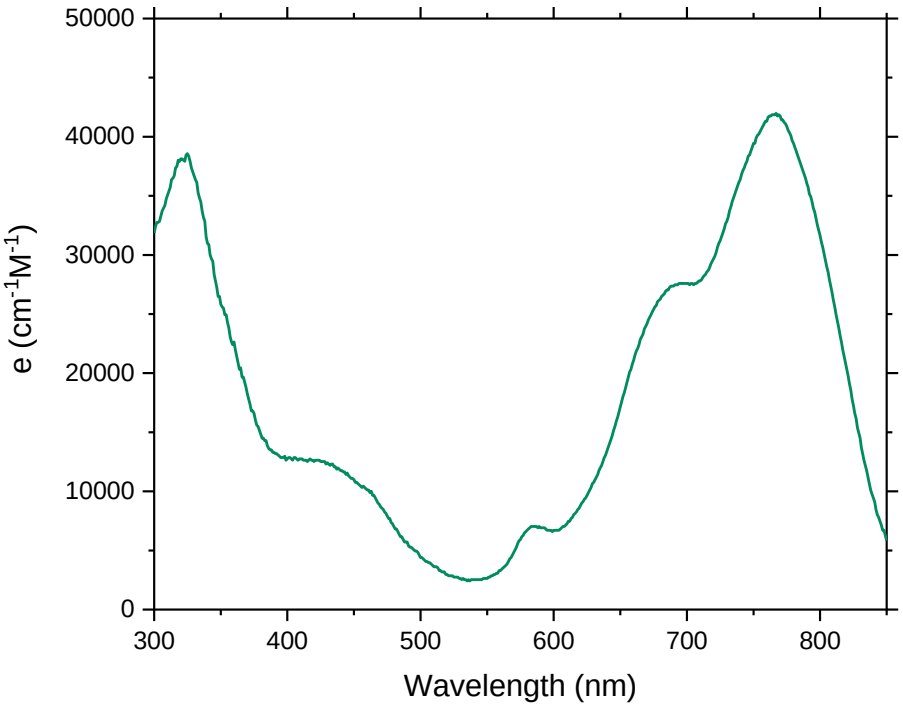

Figure S23. UV-Vis spectrum of ^{EtO}**PcFe** taken in CH_2Cl_2 (9.1 μM).

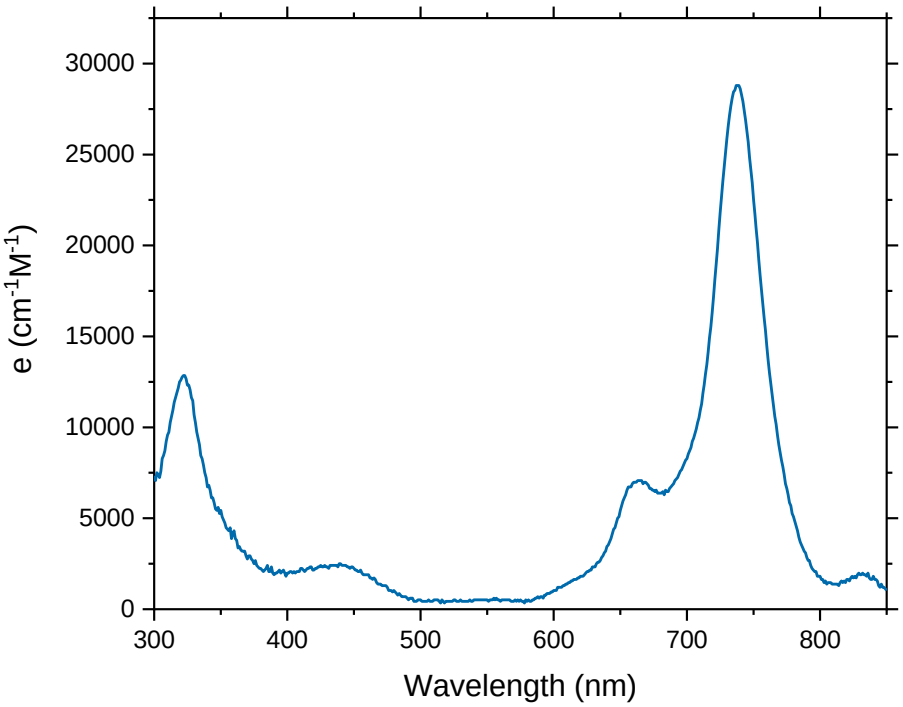

Figure S24. UV-Vis spectrum of ^{EtO}**PcCo** taken in CH_2Cl_2 (11.6 μM).

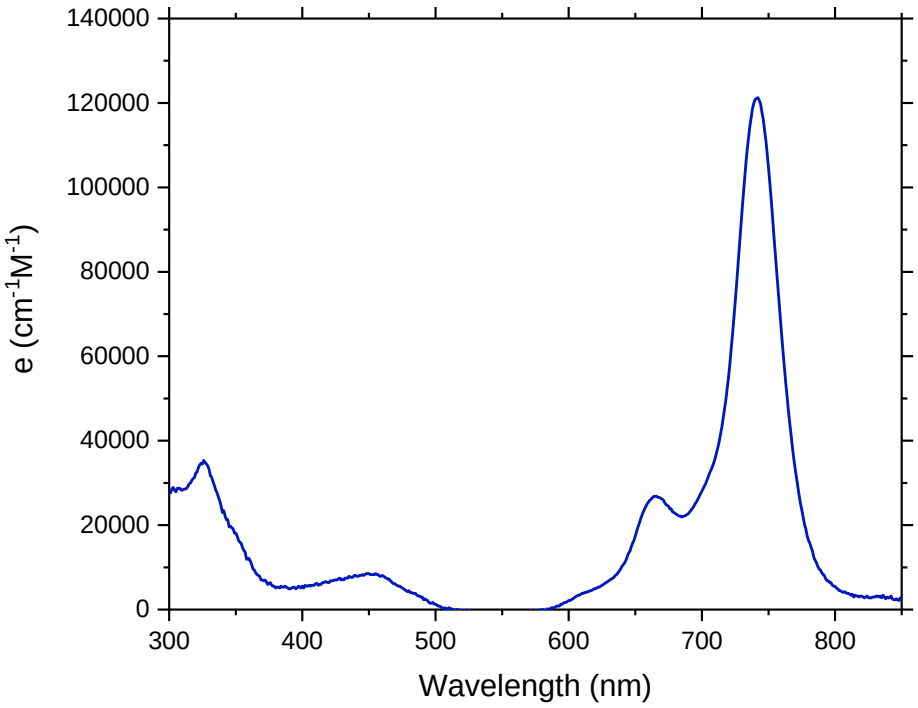

Figure S25. UV-Vis spectrum of ^{EtO}**PcNi** taken in CH_2Cl_2 (4.7 μM).

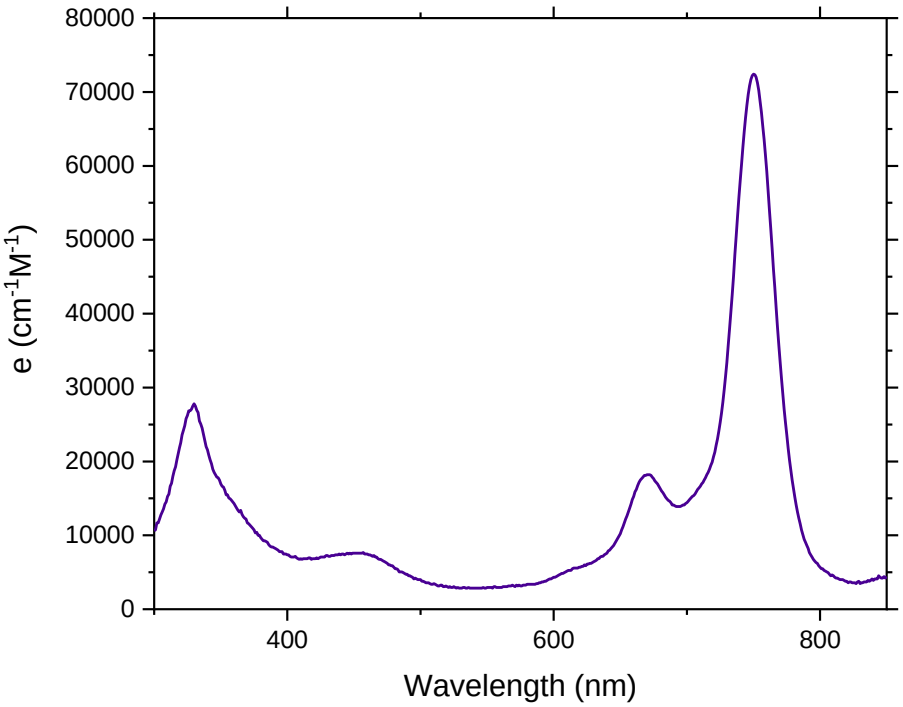

Figure S26. UV-Vis spectrum of ^{EtO}**PcCu** taken in CH_2Cl_2 (9.5 μM).

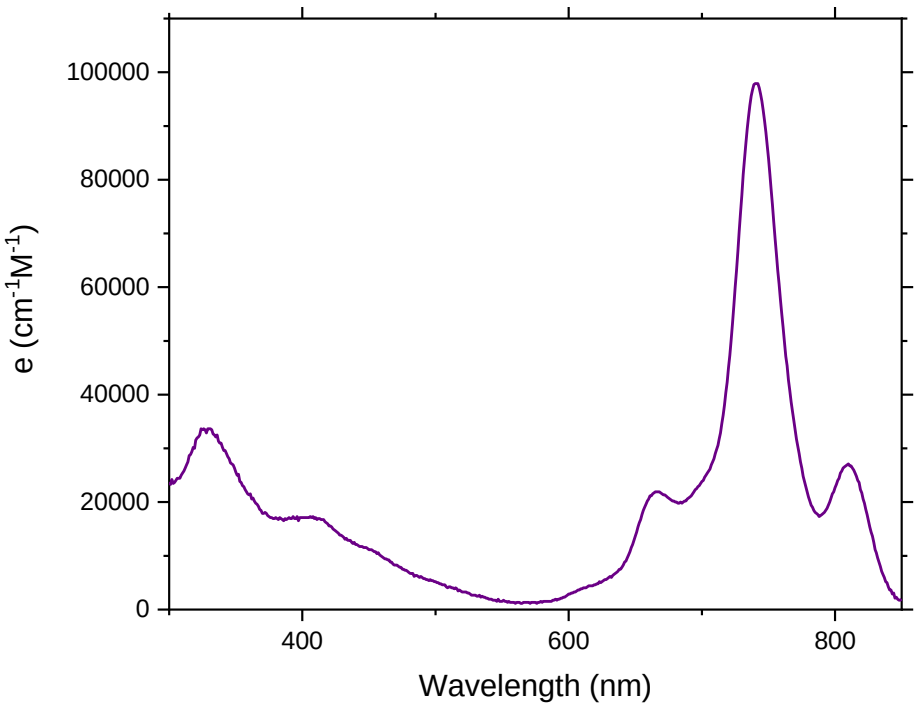

Figure S27. UV-Vis spectrum of ^{EtO}**PcZn** taken in CH_2Cl_2 (1.6 μM).

4. ^{57}Fe Mössbauer Spectrum

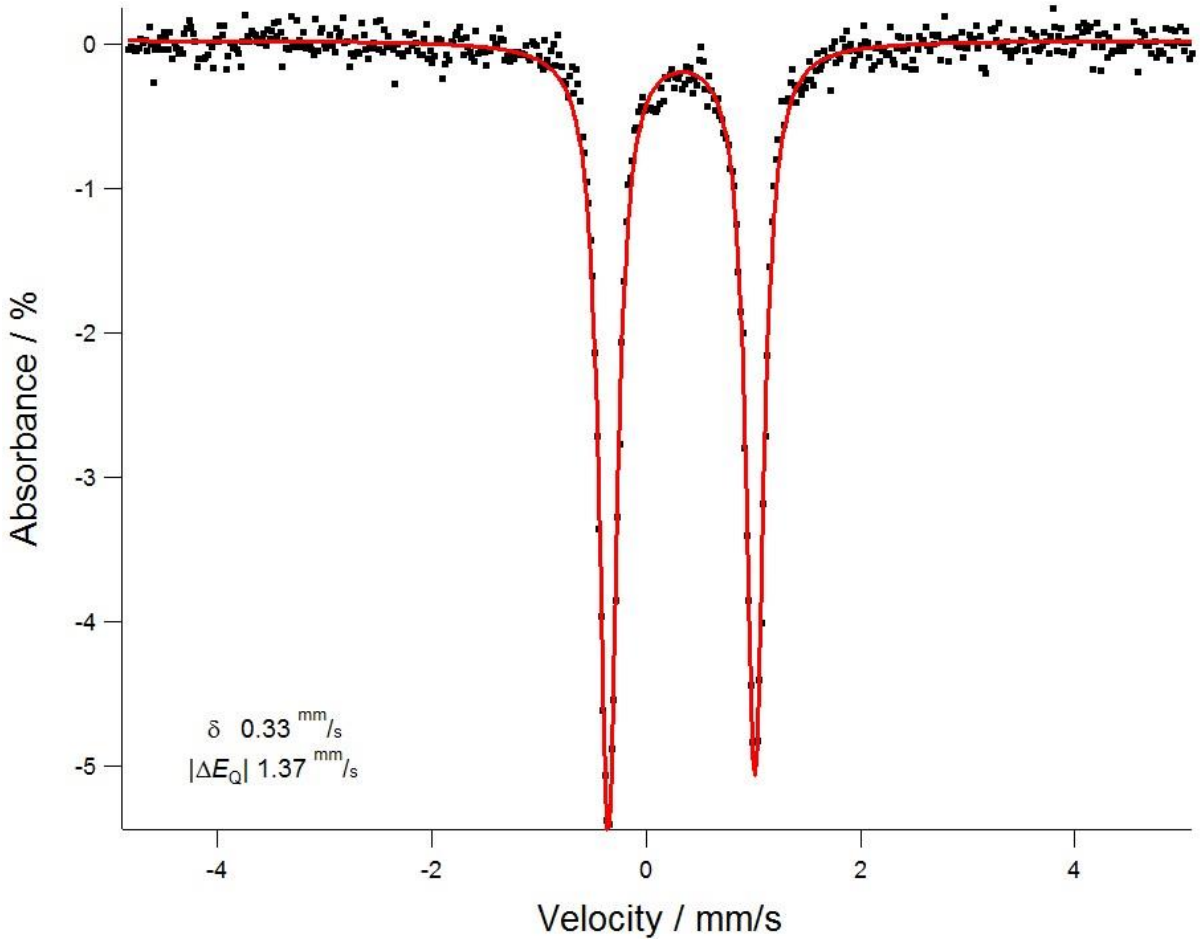

Figure S28. Zero-field ^{57}Fe Mössbauer spectrum of ^{EtO}**PcFe**, with isomer shift and quadrupole splitting values (lower left). Taken at 90 K.

5. Crystallographic Figures

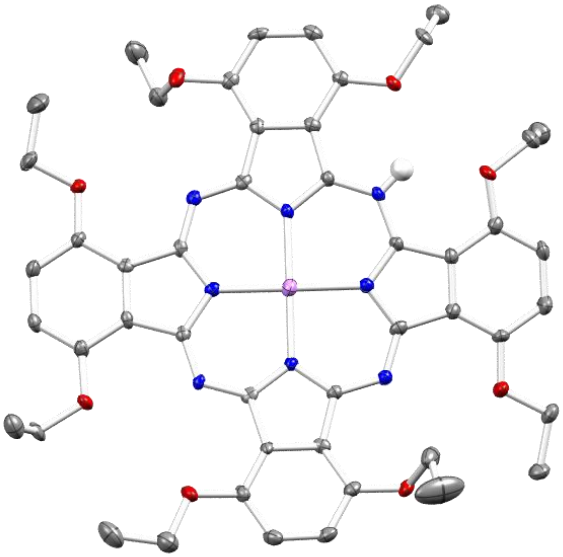

Figure S29. Solid-state molecular structure of ^{EtO}**PcHLi**. Hydrogen atoms (excluding H_{meso}) and co-crystallized solvent molecules are omitted for clarity. (C, gray; N, blue; O, red; Li, lilac; H, off-white)

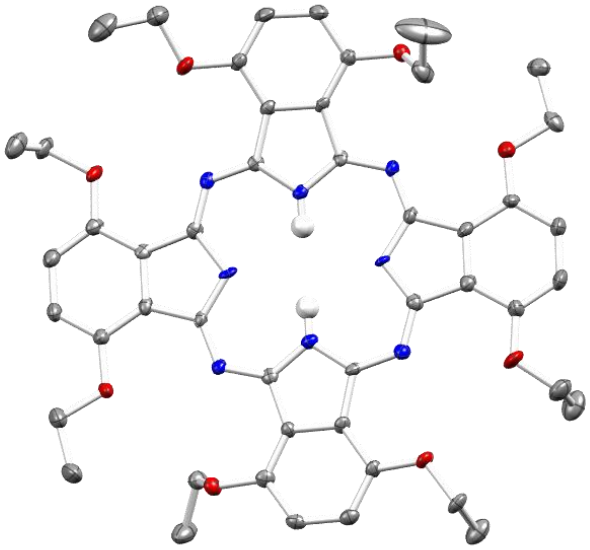

Figure S30. Solid-state molecular structure of ^{EtO}**PcH$_2$**. Hydrogen atoms (excluding H_{pyr}) and co-crystallized solvent molecules are omitted for clarity. (C, gray; N, blue; O, red; H, off-white)

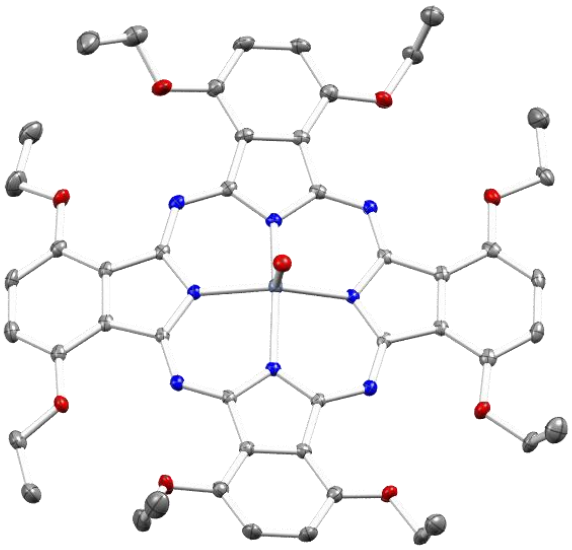

Figure S31. Solid-state molecular structure of ^{EtO}**PcVO**. Hydrogen atoms and co-crystallized solvent molecules are omitted for clarity. (C, gray; N, blue; O, red; V, slate blue)

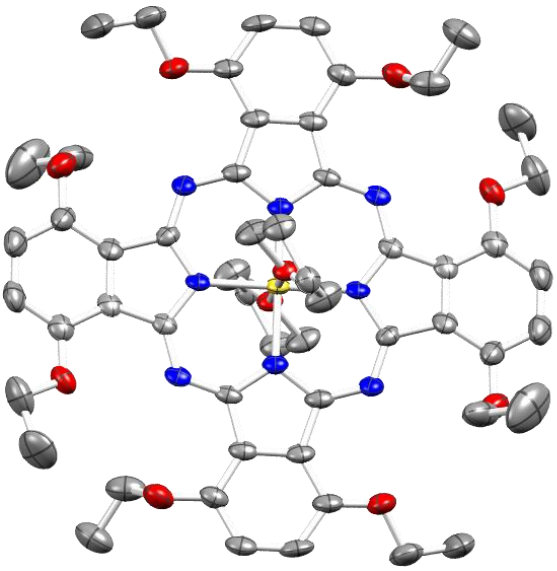

Figure S32. Solid-state molecular structure of ^{EtO}**PcCr**. Hydrogen atoms and co-crystallized solvent molecules are omitted for clarity. Only one molecule in the unit cell shown for clarity. (C, gray; N, blue; O, red; Cr, yellow)

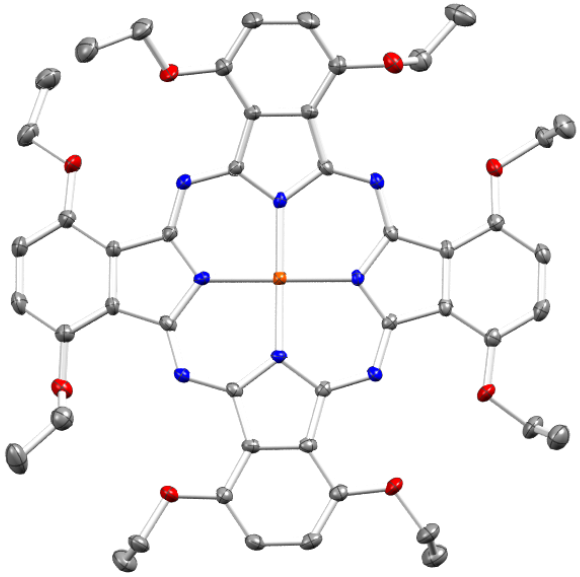

Figure S33. Solid-state molecular structure of ^{EtO}**PcFe**. Hydrogen atoms and co-crystallized solvent molecules are omitted for clarity. (C, gray; N, blue; O, red; Fe, orange)

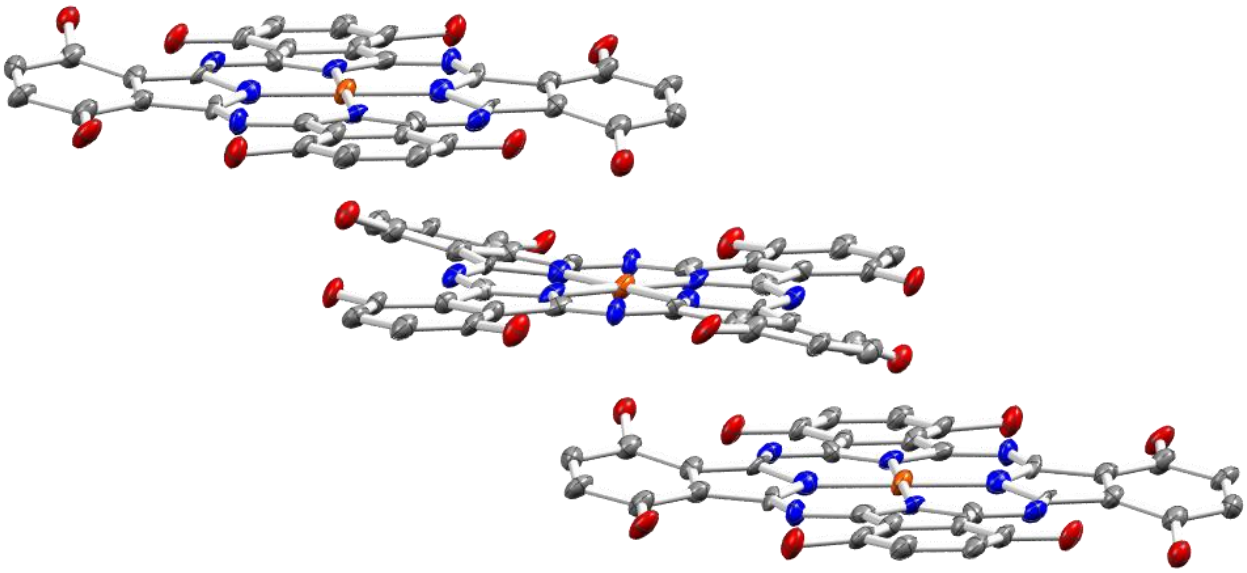

Figure S34. Extended structure of ^{EtO}**PcFe*** showing overlap of oxygen atoms from adjacent macrocycles with Fe centers. Hydrogen atoms, ethyl groups, and co-crystallized solvent molecules are omitted for clarity. (C, gray; N, blue; O, red; Fe, orange)

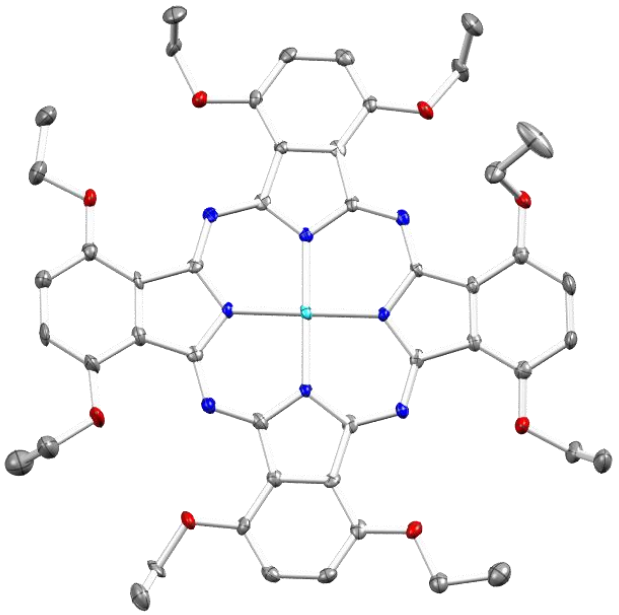

Figure S35. Solid-state molecular structure of ^{EtO}**PcCo**. Hydrogen atoms and co-crystallized solvent molecules are omitted for clarity. (C, gray; N, blue; O, red; Co, aquamarine)

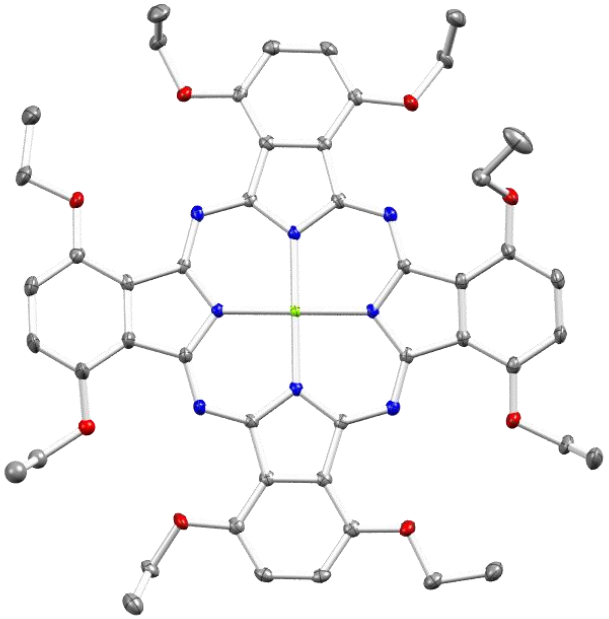

Figure S36. Solid-state molecular structure of ^{EtO}**PcNi**. Hydrogen atoms and co-crystallized solvent molecules are omitted for clarity. (C, gray; N, blue; O, red; Ni, lime green)

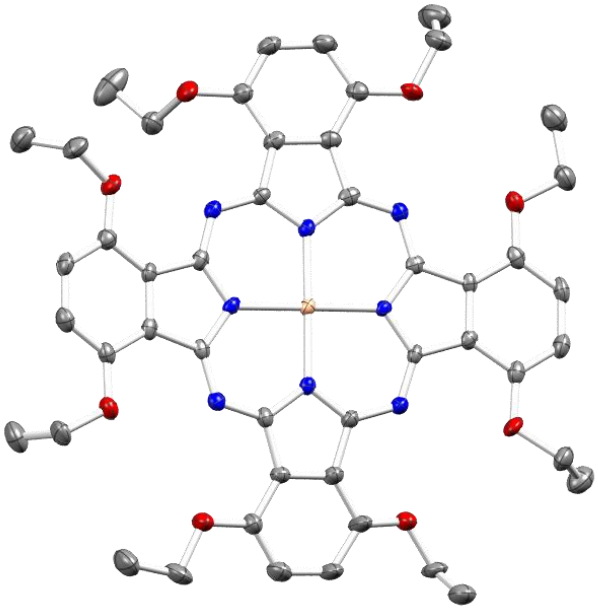

Figure S37. Solid-state molecular structure of ^{EtO}**PcCu**. Hydrogen atoms and co-crystallized solvent molecules are omitted for clarity. (C, gray; N, blue; O, red; Cu, gold)

Tables S1. Calculated peripheral C_x-to-N_4 distances (x = 1-8) as shown in Fig. 2 of the paper with N_4 defined as the plane created by the four inner pyrrolic nitrogen atoms in the Pc macrocycle. For unit cells containing multiple ^{EtO}**PcM** molecules, the second set of values are shown in parentheses. All d values are in Å and all dihedral angles in degrees (°).

Compd.	|*d*| (C_1–N_4)	|*d*| (C_2–N_4)	|*d*| (C_3–N_4)	|*d*| (C_4–N_4)	|*d*| (C_5–N_4)	|*d*| (C_6–N_4)	|*d*| (C_7–N_4)	|*d*| (C_8–N_4)	d_{avg}	M–N_4 dist.	|dihed.$_1$|	|dihed.$_2$|	|dihed.$_{avg}$|	$d_{iso\text{-}N4}$
^{OEt}**PcH$_2$**	*0.779*	*0.704*	*0.687*	*0.477*	*0.013*	*0.076*	*0.217*	*0.177*	*0.391*	*N/A*	*11.4*	*13.6*	*12.5*	*3.376*
^{OEt}**PcLiH**	*0.114*	*0.064*	*0.898*	*0.804*	*0.752*	*0.574*	*0.037*	*0.123*	*0.421*	*0.077*	*12.9*	*12.3*	*12.6*	*3.398*
^{OEt}**PcVO**	*1.243*	*1.321*	*0.171*	*0.083*	*0.130*	*0.112*	*0.496*	*0.581*	*0.517*	*0.557*	*15.2*	*9.0*	*12.1*	*3.266*
^{OEt}**PcCr**	*0.276*	*0.245*	*0.236*	*0.051*	*0.276*	*0.245*	*0.236*	*0.051*	*0.202*	*0*	*0*	*0*	*0*	*N/A*
	(0.425)	*(0.203)*	*(0.024)*	*(0.036)*	*(0.425)*	*(0.203)*	*(0.024)*	*(0.036)*	*(0.172)*	*(0)*	*(0)*	*(0)*	*(0)*	
^{OEt}**PcMnCl**	*0.651*	*0.616*	*0.253*	*0.245*	*0.126*	*0.180*	*0.252*	*0.335*	*0.332*	*0.260*	*6.6*	*7.5*	*7.1*	*3.372*
^{OEt}**PcMnN**	*0.389*	*0.298*	*0.156*	*0.074*	*0.443*	*0.559*	*0.919*	*0.926*	*0.471*	*0.402*	*11.0*	*10.5*	*10.8*	*3.296*
	(0.225)	*(0.262)*	*(0.616)*	*(0.622)*	*(0.393)*	*(0.247)*	*(0.063)*	*(0.135)*	*(0.320)*	*(0.407)*	*(7.9)*	*(6.9)*	*(7.4)*	
^{OEt}**PcFe**	*0.162*	*0.162*	*1.250*	*1.244*	*1.244*	*1.250*	*0.162*	*0.162*	*0.705*	*0*	*17.5*	*17.5*	*17.5*	*3.265*
^{OEt}**PcFe***	*0.109*	*0.350*	*0.256*	*0.243*	*0.109*	*0.350*	*0.256*	*0.243*	*0.240*	*0*	*0*	*0*	*0*	*N/A*
^{OEt}**PcCo**	*0.888*	*0.699*	*0.847*	*0.800*	*0.390*	*0.172*	*0.058*	*0.008*	*0.483*	*0.018*	*18.8*	*9.7*	*14.3*	*3.332*
^{OEt}**PcNi**	*0.347*	*0.110*	*0.002*	*0.031*	*0.699*	*0.602*	*0.786*	*0.742*	*0.415*	*0.009*	*15.4*	*9.7*	*12.6*	*3.401*
^{OEt}**PcCu**	*0.782*	*0.812*	*0.666*	*0.779*	*0.030*	*0.070*	*0.134*	*0.329*	*0.450*	*0.024*	*9.6*	*15.7*	*12.7*	*3.380*

6. Electrochemical Figures

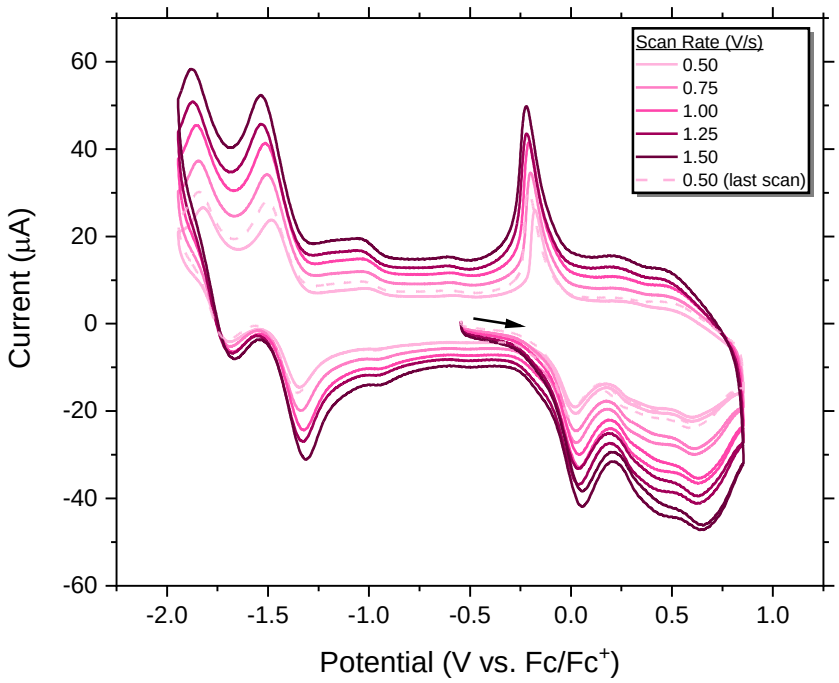

Figure S38. CVs of ^{EtO}**PcH$_2$** at varying scan rates (inset) with the arrow indicating initial scan direction. Experimental conditions: Taken in DCM with 0.53 mM of ^{EtO}**PcH$_2$**, 0.1 M of [Bu$_4$N][PF$_6$], 3 mm diameter glassy carbon working electrode, Pt wire counter electrode, and Pt wire pseudo-reference electrode. Internally referenced to Fc/Fc$^+$.

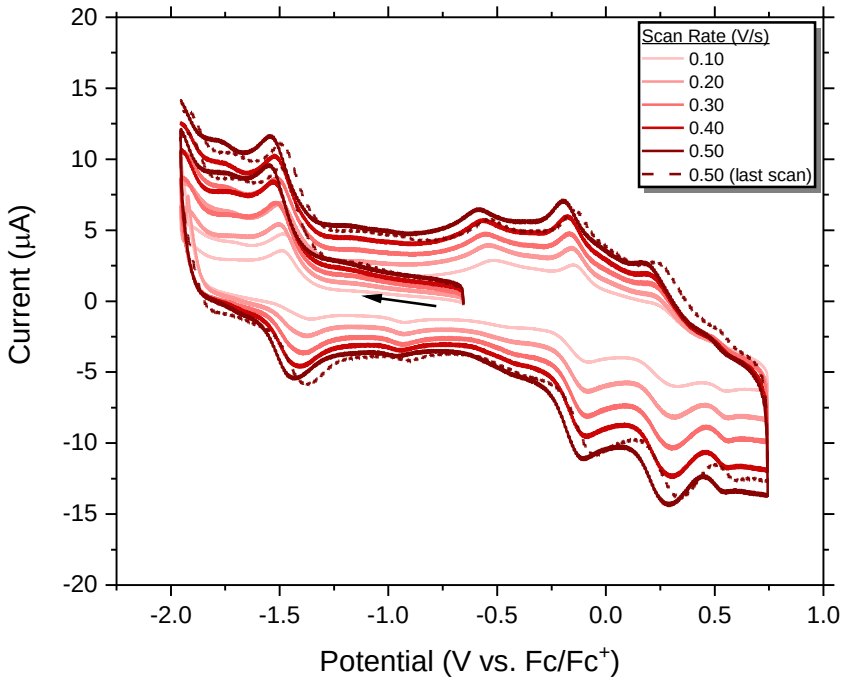

Figure S39. CVs of ^{EtO}**PcHLi** at varying scan rates (inset) with the arrow indicating initial scan direction. Experimental conditions: Taken in DCM with 0.53 mM of ^{EtO}**PcLiH**, 0.1 M of [Bu$_4$N][PF$_6$], 3 mm diameter glassy carbon working electrode, Pt wire counter electrode, and Pt wire pseudo-reference electrode. Internally referenced to Fc/Fc$^+$.

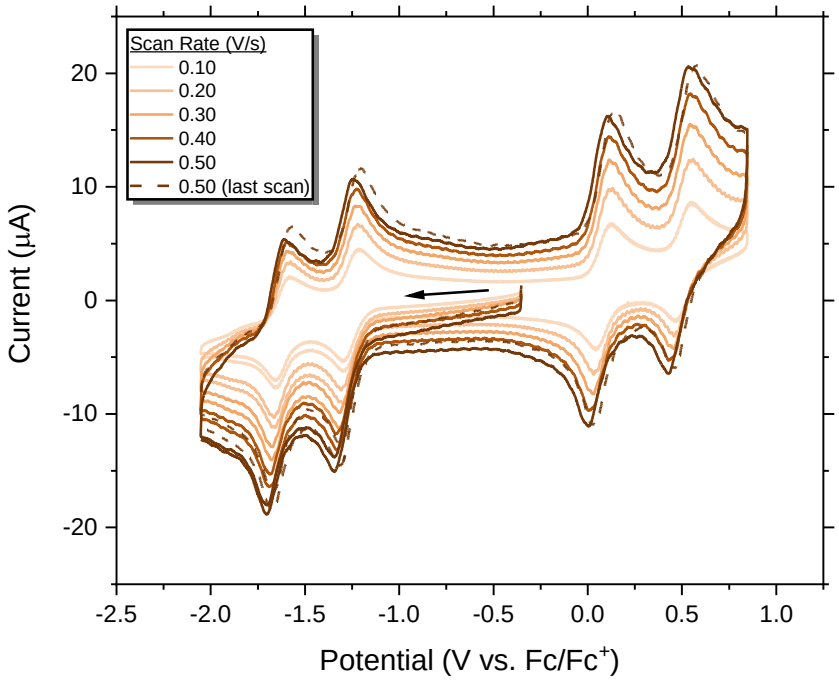

Figure S40. CVs of ^{EtO}**PcVO** at varying scan rates (inset) with the arrow indicating initial scan direction. Experimental conditions: Taken in DCM with 0.45 mM of ^{EtO}**PcVO**, 0.1 M of [Bu_4N][PF_6], 3 mm diameter glassy carbon working electrode, Pt wire counter electrode, and Pt wire pseudo-reference electrode. Internally referenced to Fc/Fc^+.

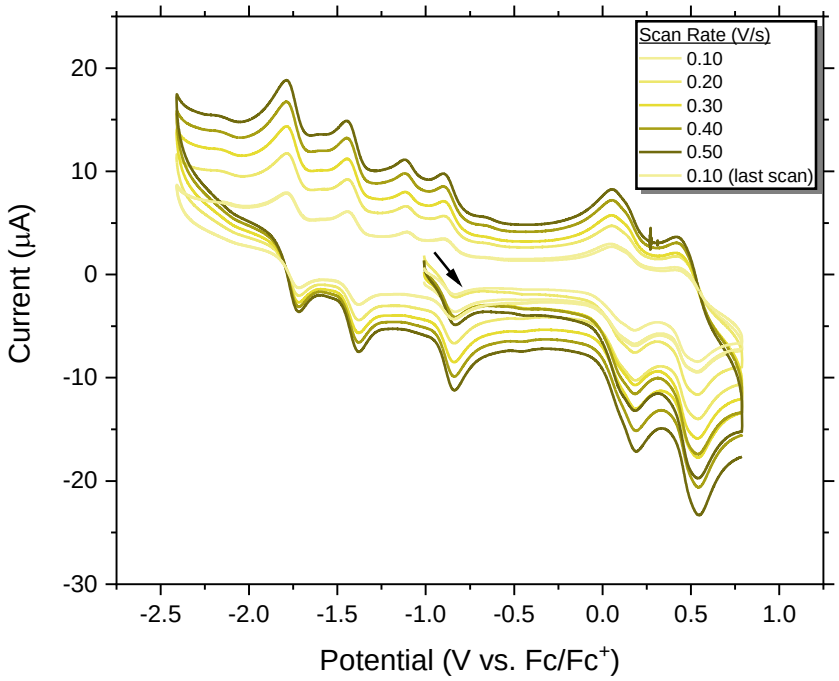

Figure S41. CVs of ^{EtO}**PcCr** at varying scan rates (inset) with the arrow indicating initial scan direction. Experimental conditions: Taken in acetonitrile with 0.52 mM of ^{EtO}**PcCr**, 0.1 M of [Bu_4N][PF_6], 3 mm diameter glassy carbon working electrode, Pt wire counter electrode, and Pt wire pseudo-reference electrode. Internally referenced to Fc/Fc^+.

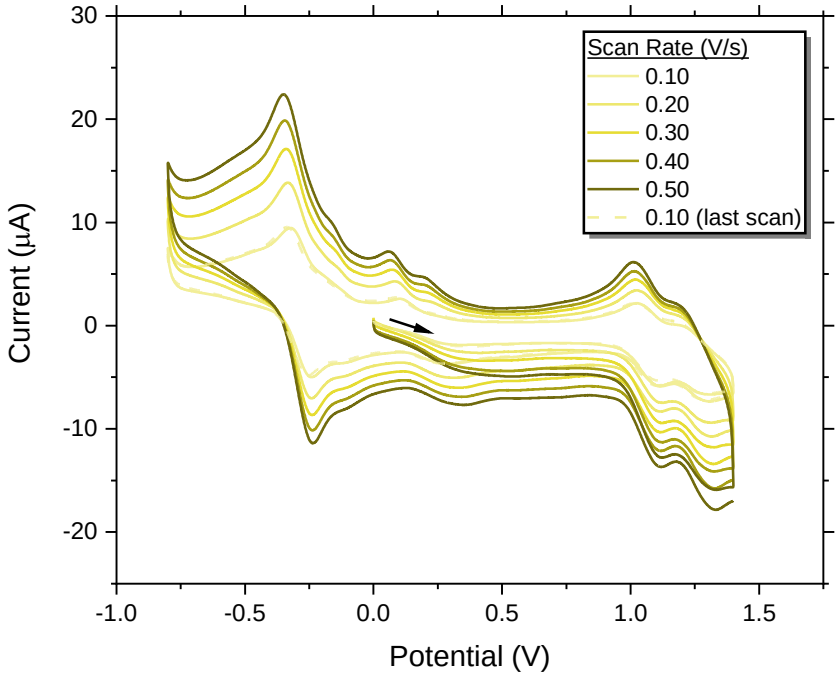

Figure S42. CVs of ^{EtO}**PcCr** at varying scan rates (inset) with the arrow indicating initial scan direction. Experimental conditions: Taken in DCM with 0.57 mM of ^{EtO}**PcCr**, 0.1 M of $[Bu_4N][PF_6]$, 3 mm diameter glassy carbon working electrode, Pt wire counter electrode, and Pt wire pseudo-reference electrode. Pseudo-referenced to a Pt wire electrode.

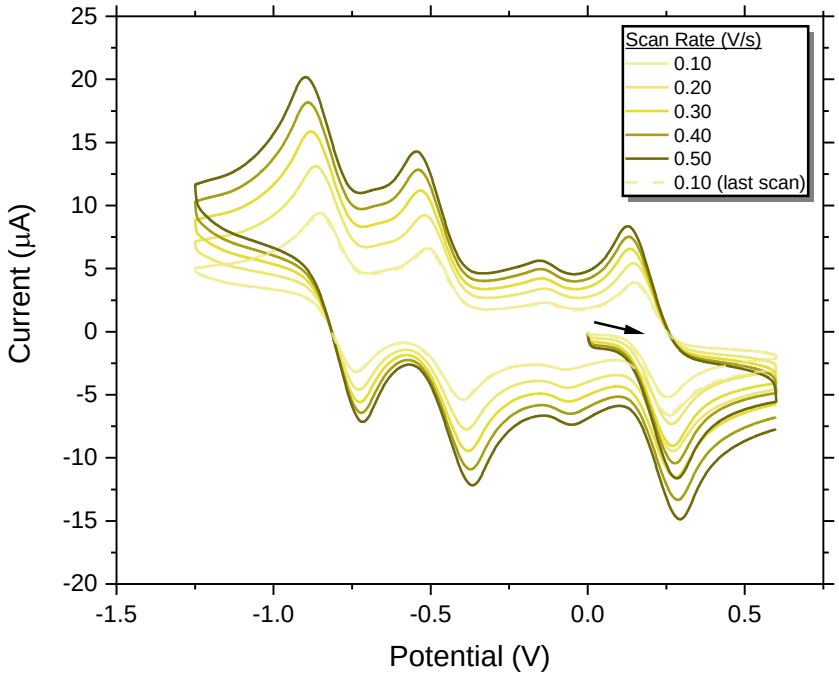

Figure S43. CVs of ^{EtO}**PcCr** at varying scan rates (inset) with the arrow indicating initial scan direction. Experimental conditions: Taken in THF with 0.52 mM of ^{EtO}**PcCr**, 0.1 M of $[Bu_4N][PF_6]$, 3 mm diameter glassy carbon working electrode, Pt wire counter electrode, and Pt wire pseudo-reference electrode. Pseudo-referenced to a Pt wire electrode.

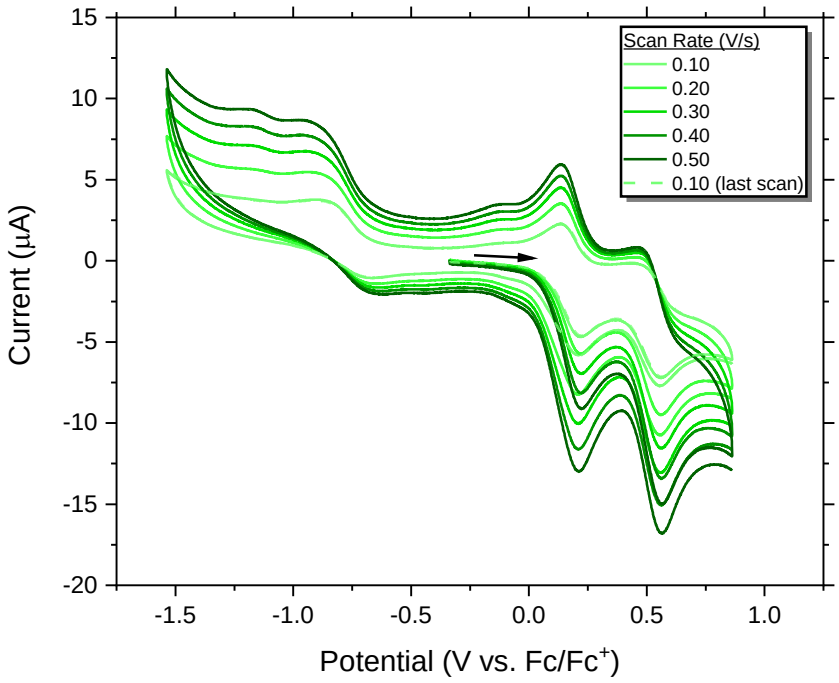

Figure S44. CVs of ^{EtO}**PcMnCl** at varying scan rates (inset) with the arrow indicating initial scan direction. Experimental conditions: Taken in DCM with 0.50 mM of ^{EtO}**PcMnCl**, 0.1 M of $[Bu_4N][PF_6]$, 3 mm diameter glassy carbon working electrode, Pt wire counter electrode, and Pt wire pseudo-reference electrode. Internally referenced to Fc/Fc^+.

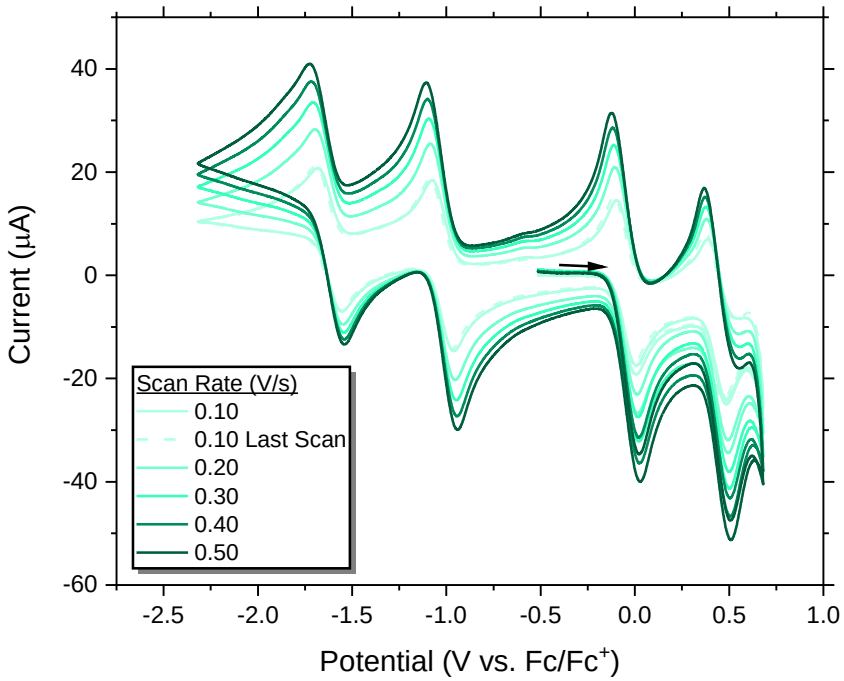

Figure S45. CVs of ^{EtO}**PcFe** at varying scan rates (inset) with the arrow indicating initial scan direction. Experimental conditions: Taken in THF with 0.43 mM of ^{EtO}**PcFe**, 0.1 M of $[Bu_4N][PF_6]$, 3 mm diameter glassy carbon working electrode, Pt wire counter electrode, and Pt wire pseudo-reference electrode. Internally referenced to Fc/Fc^+.

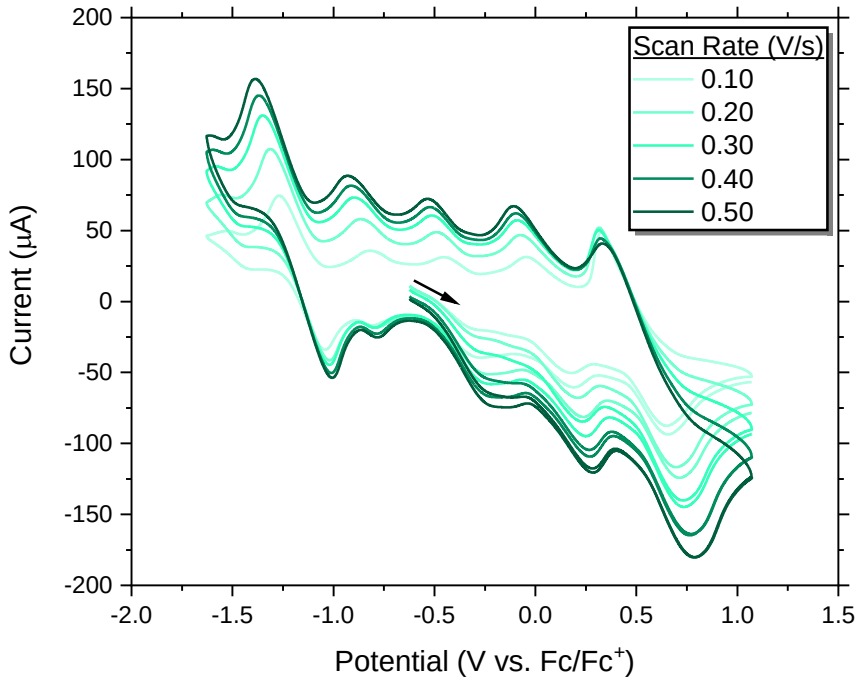

Figure S46. CVs of ^{EtO}**PcFe** at varying scan rates (inset) with the arrow indicating initial scan direction. Experimental conditions: Taken in DCM with 0.50 mM of ^{EtO}**PcFe**, 0.1 M of $[Bu_4N][PF_6]$, 3 mm diameter glassy carbon working electrode, Pt wire counter electrode, and Pt wire pseudo-reference electrode. Internally referenced to Fc/Fc^+.

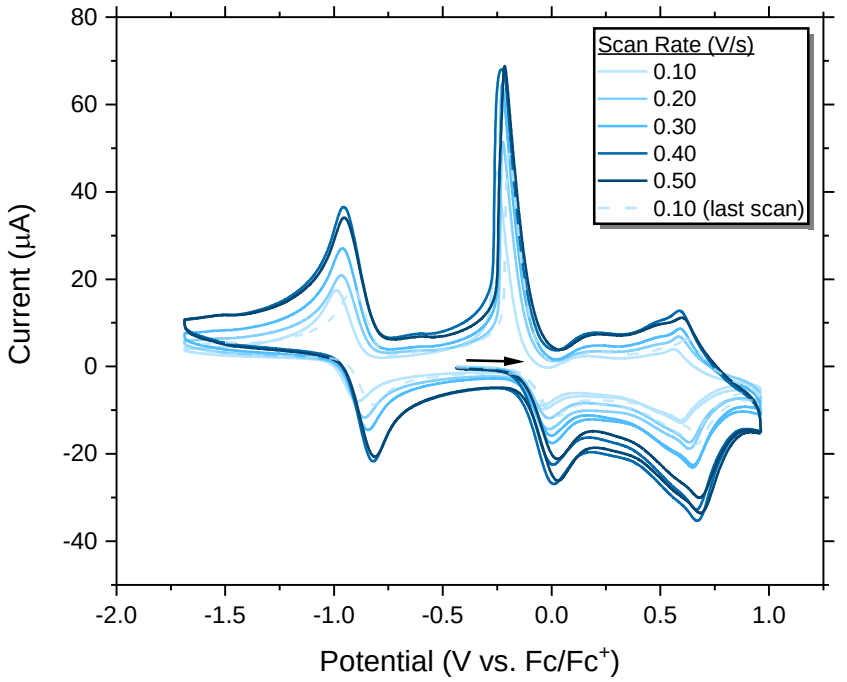

Figure S47. CVs of ^{EtO}**PcCo** at varying scan rates (inset) with the arrow indicating initial scan direction. Experimental conditions: Taken in DCM with 0.54 mM of ^{EtO}**PcCo**, 0.1 M of $[Bu_4N][PF_6]$, 3 mm diameter glassy carbon working electrode, Pt wire counter electrode, and Pt wire pseudo-reference electrode. Internally referenced to Fc/Fc^+.

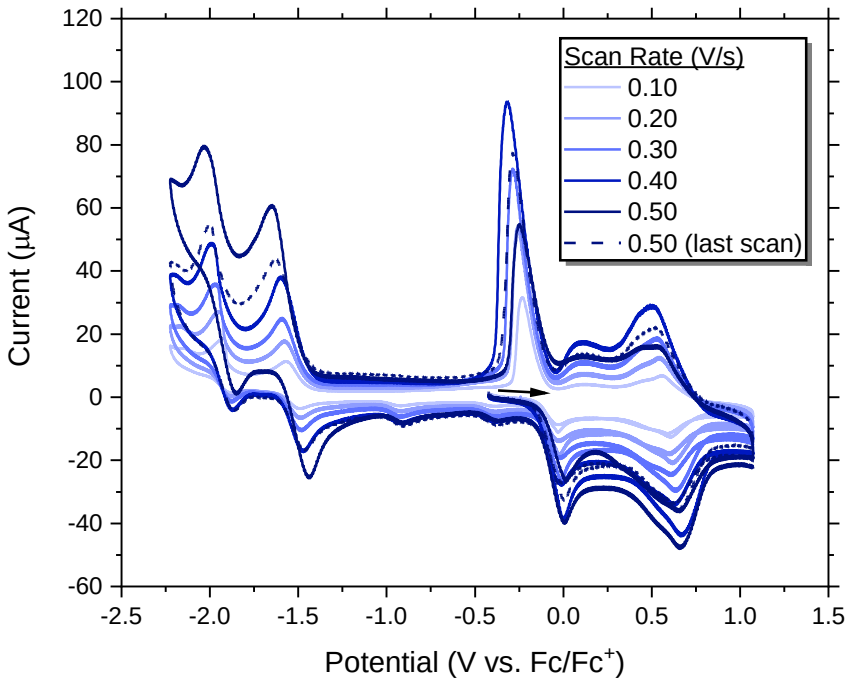

Figure S48. CVs of ^{EtO}**PcNi** at varying scan rates (inset) with the arrow indicating initial scan direction. Experimental conditions: Taken in DCM with 0.48 mM of ^{EtO}**PcNi**, 0.1 M of $[Bu_4N][PF_6]$, 3 mm diameter glassy carbon working electrode, Pt wire counter electrode, and Pt wire pseudo-reference electrode. Internally referenced to Fc/Fc^+.

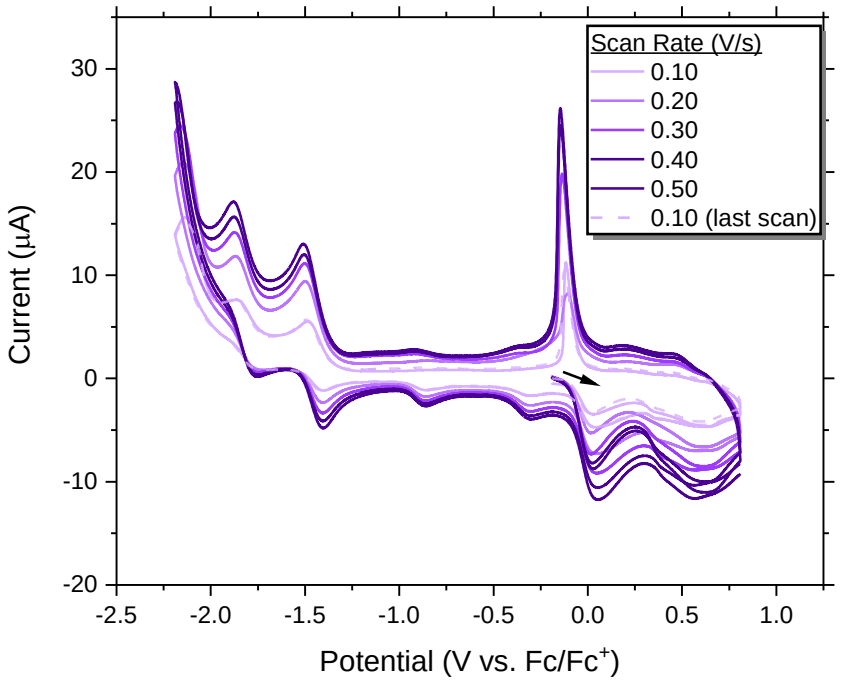

Figure S49. CVs of ^{EtO}**PcCu** at varying scan rates (inset) with the arrow indicating initial scan direction. Experimental conditions: Taken in DCM with 0.48 mM of ^{EtO}**PcCu**, 0.1 M of $[Bu_4N][PF_6]$, 3 mm diameter glassy carbon working electrode, Pt wire counter electrode, and Pt wire pseudo-reference electrode. Internally referenced to Fc/Fc^+.

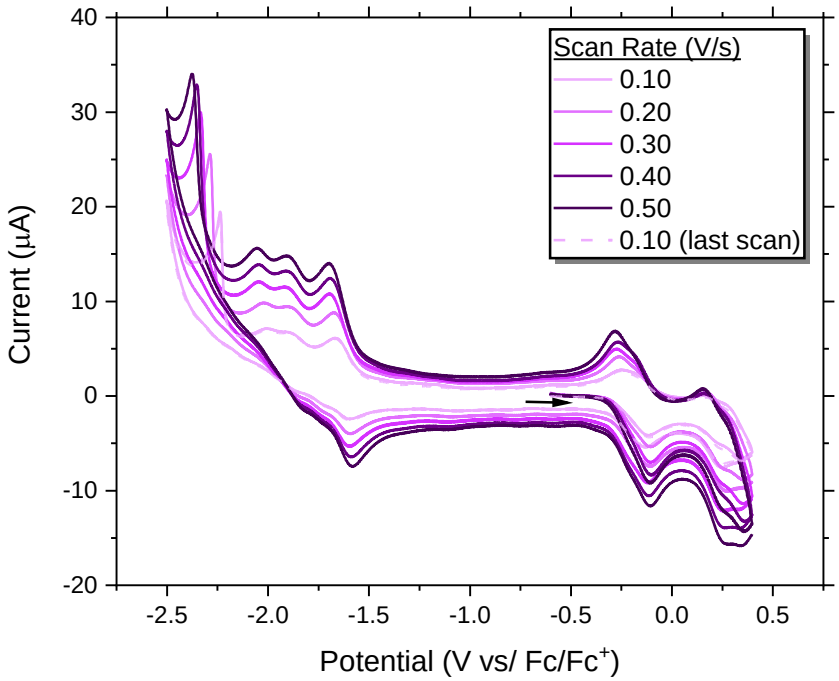

Figure S50. CVs of ^{EtO}**PcZn** at varying scan rates (inset) with the arrow indicating initial scan direction. Experimental conditions: Taken in DCM with 0.60 mM of ^{EtO}**PcZn**, 0.1 M of $[Bu_4N][PF_6]$, 3 mm diameter glassy carbon working electrode, Pt wire counter electrode, and Pt wire pseudo-reference electrode. Internally referenced to Fc/Fc^+.